https://doi.org/10.5194/egusphere-2024-2159
Preprint. Discussion started: 25 July 2024

Wind-driven Emission of Marine Ice Nucleating Particles in the Scripps Ocean-Atmosphere Research Simulator (SOARS)

Kathryn A. Moore[1,*], Thomas C. J. Hill[1], Samantha Greeney[2,^], Chamika K. Madawala[3], Raymond J. Leibensperger III[4], Christopher D. Cappa[5], M. Dale Stokes[4], Grant B. Deane[4], Christopher Lee[4], Alexei V. Tivanski[3], Kimberly A. Prather[4,6], and Paul J. DeMott[1]

[1]Department of Atmospheric Science, Colorado State University, Fort Collins, CO, USA
[2]Department of Atmospheric Sciences, Texas A&M University, College Station, TX, USA
[3]Department of Chemistry, University of Iowa, Iowa City, IA, USA
[4]Scripps Institution of Oceanography, University of California San Diego, La Jolla, CA, USA
[5]Department of Civil and Environmental Engineering, University of California Davis, Davis, CA, USA
[6]Department of Chemistry and Biochemistry, University of California San Diego, La Jolla, CA, USA
[*]Now at: Earth System Science Interdisciplinary Center, University of Maryland, College Park, and NASA Goddard Space Flight Center, Greenbelt, MD, USA
[^]Now at: Department of Atmospheric Science, Colorado State University, Fort Collins, CO, USA

Correspondence: Kathryn A. Moore (kathryn.a.moore@colostate.edu)

Abstract. Sea spray aerosol (SSA) represent one of the most abundant natural aerosol types, contributing significantly to global aerosol mass and aerosol optical depth, as well as to both the magnitude and uncertainty of aerosol radiative forcing. In addition to their direct effects, SSA can also serve as ice nucleating particles (INPs), which are required for the initiation of cloud glaciation at temperatures warmer than ∼-36 °C. This study presents initial results from the CHaracterizing Atmosphere-Ocean parameters in SOARS (CHAOS) mesocosm campaign, which was conducted in the new Scripps Ocean-Atmosphere Research Simulator (SOARS) wind-wave channel at the Scripps Institution of Oceanography. SOARS allows for isolation of individual factors, such as wave height, wind speed, water temperature, or biological state, and can carefully vary them in a controlled manner. Here, we focus on the influence of wind speed on the emission of SSA and INPs. Unlike recent measurements from the Southern Ocean, real-time and offline INP observations during CHAOS exhibited opposite relationships with wind speed, which may be related to sampling inlet differences. Changes in the INP activated fraction, dominant INP particle morphology, and INP composition were seen to vary with wind. Seawater ice nucleating entity concentrations during CHAOS were stable over time, indicating changes in atmospheric INPs were driven by wind speed and wave-breaking mechanics rather than variations in seawater chemistry or biology. While specific emission mechanisms remain elusive, these observations may help explain some of the variability in INP concentration and composition that have been seen in ambient measurements.

1 Introduction

Sea spray aerosol (SSA) are marine-derived particles composed of mixtures of inorganic salts and organic compounds, with the exact composition and mixing state varying based on particle size, production mechanism, and the underlying biology and geochemistry of the source seawater (e.g. Lewis and Schwartz, 2004; O'Dowd and de Leeuw, 2007; de Leeuw et al.,

https://doi.org/10.5194/egusphere-2024-2159
Preprint. Discussion started: 25 July 2024

2011; Cochran et al., 2017). Along with mineral and soil dusts, SSA dominates atmospheric aerosol mass, and contributes ~30 % to globally-averaged total aerosol optical depth (AOD) (O'Dowd and de Leeuw, 2007; Bellouin et al., 2013). SSA are generated through wind stress at the ocean surface, either through the direct tearing of breaking wave crests (spume drops) or as a result of bubble bursting (film and jet drops) following air entrainment during wave breaking (Lewis and Schwartz, 2004; O'Dowd and de Leeuw, 2007; Deike et al., 2022). Additionally, oxidation of dimethyl sulfide (DMS) and other biogenic volatile organic compounds (BVOCs) emitted from the ocean can lead to the condensation of gas-phase species and formation of secondary marine aerosol (SMA) (Lewis and Schwartz, 2004; Quinn et al., 2017; Naik et al., 2021). Given their ubiquity in the atmosphere, SSA are an important contributor to both the magnitude and uncertainty of aerosol radiative forcing (Andreae, 2007; Carslaw et al., 2013, 2017; Forster et al., 2021).

The indirect radiative impact of both SSA and SMA through their role as cloud condensation nuclei (CCN) has received considerable attention from observational, laboratory, and modeling studies (e.g. Pierce and Adams, 2006; Andreae, 2007; Grythe et al., 2014; Modini et al., 2015; McCoy et al., 2015a; Quinn et al., 2017; Heinze et al., 2019; Mayer et al., 2020; Gryspeerdt et al., 2023). Spurred by observations in remote ocean regions and laboratory mesocosm studies (Rosinski et al., 1987; Bigg, 1973, 1990; Knopf et al., 2011; DeMott et al., 2016), the contribution of marine aerosol to the ice nucleating particle (INP) budget, and thus indirectly to cloud phase, has come under increasing focus in recent years (e.g. Burrows et al., 2013; Wilson et al., 2015; Irish et al., 2017; Vergara-Temprado et al., 2017, 2018; McCluskey et al., 2018c, b, a; Welti et al., 2018; Huang et al., 2018; Creamean et al., 2019; McCluskey et al., 2019; Schmale et al., 2019; Irish et al., 2019; Welti et al., 2020; Ickes et al., 2020; Hartmann et al., 2020, 2021; Zhao et al., 2021; Mitts et al., 2021; Tatzelt et al., 2022; Alpert et al., 2022; Steinke et al., 2022; Raatikainen et al., 2022; Lin et al., 2022; McCluskey et al., 2023; Raman et al., 2023; Miyakawa et al., 2023; Kawana et al., 2024). INPs are critical in initiating cloud glaciation at temperatures warmer than ~-36 °C and thus exert a large influence on cloud properties related to phase, such as lifetime, precipitation formation, and radiative forcing (e.g. Kanji et al., 2017). Additionally, mixed-phase clouds, which contain both liquid and ice, play major roles in determining cloud feedbacks (McCoy et al., 2015b, 2016), global cloud radiative properties (Cesana and Storelvmo, 2017), and equilibrium climate sensitivity (Zelinka et al., 2020; Bjordal et al., 2020).

Measurements of ice nucleation in marine environments were first made in the late 1950s and 1960s (see Ickes et al., 2020, Table 1). Since then, a few studies have suggested whole phytoplankton cells or marine bacteria may be the ice nucleating components of SSA (Fall and Schnell, 1985; Knopf et al., 2011; Wilbourn et al., 2020; Beall et al., 2021). However, the majority of studies indicate marine macromolecules, phytoplankton exudates, or other biogenic, organic species are the ice nucleating components based on the generally small size (<0.2 μm) of ice nucleating entities in seawater, and their relationship with biological activity (Schnell and Vali, 1976; Rosinski et al., 1987; Knopf et al., 2011; Wilson et al., 2015; Wang et al., 2015; Ladino et al., 2016; DeMott et al., 2016; Irish et al., 2017; McCluskey et al., 2018b; Alpert et al., 2022; Hill et al., 2023). Based on laboratory and mesocosm experiments, several studies have also inferred different components may be active at different temperatures, as well as at different times throughout the onset and decay of phytoplankton blooms (DeMott et al., 2016; McCluskey et al., 2018b; Ickes et al., 2020). In addition to the small and ubiquitous marine organic INPs, a second category of more intermittent, larger, and heat sensitive marine INPs that are active at warmer temperatures has been identified

https://doi.org/10.5194/egusphere-2024-2159
Preprint. Discussion started: 25 July 2024

(McCluskey et al., 2018b; Ickes et al., 2020; Hartmann et al., 2020; van Pinxteren et al., 2020). These may be associated with microbes or cellular debris, but have not been definitively identified. Recent laboratory studies have pointed to the importance of supermicron SSA as a marine INP (Mitts et al., 2021), however, no assessment of the atmospheric transport of such particles was conducted and ambient observations have yet to confirm this.

INP concentrations in remote marine regions are generally several orders of magnitude lower than those in continental areas (DeMott et al., 2016; McCluskey et al., 2018c; Welti et al., 2020; Tatzelt et al., 2022). Based on normalization by particle number or surface area, marine INPs are also significantly less efficient at nucleating ice than species such as mineral or soil dusts (DeMott et al., 2016; Kanji et al., 2017; McCluskey et al., 2018c). Despite this, in remote areas such as the Southern Ocean, marine INPs are hypothesized to be the dominant contributor to the INP budget due to the lack of continental influence (Burrows et al., 2013; Vergara-Temprado et al., 2017, 2018; McCluskey et al., 2019), and may dominate seasonally or intermittently in other regions such as the high Arctic (Huang et al., 2018; Creamean et al., 2019; Hartmann et al., 2020; Ickes et al., 2020; Hartmann et al., 2021). Atmospheric concentrations of the small, organic marine INP type were parameterized using observations from Mace Head in the North Atlantic (McCluskey et al., 2018c), and subsequent implementation in CAM5 (Community Atmosphere Model version 5) and CAM6 (version 6) compared well to observations made in the Southern Ocean (McCluskey et al., 2019, 2023). Other recent modeling work has focused on the intermittent, high temperature marine INPs (Steinke et al., 2022), or freezing kinetics of background SSA particles (Alpert et al., 2022). Despite these efforts, the fundamental factors controlling the emission of marine INPs from the sea surface to the atmosphere remain largely unknown.

Significantly more is known about the factors influencing the production of sea spray, although there is still huge variability in simulated SSA fluxes among models, especially in polar regions (de Leeuw et al., 2011; Grythe et al., 2014; Deike et al., 2022; Lapere et al., 2023). Numerous parameterizations for sea spray size distribution functions have been proposed (e.g. Monahan and Muircheartaigh, 1980; Monahan et al., 1986; Gong, 2003; Mårtensson et al., 2003; Lewis and Schwartz, 2004; de Leeuw et al., 2011; Sofiev et al., 2011; Jaeglé et al., 2011; Meskhidze et al., 2013; Ovadnevaite et al., 2014; Grythe et al., 2014; Salter et al., 2015), with the choice influencing not only emitted SSA number and mass, but also the simulated radiative budget and aerosol-cloud interactions once implemented in models (Grythe et al., 2014; McCoy et al., 2015a; Barthel et al., 2019; Johnson et al., 2020). Although wind speed is the dominant influence on SSA production (Lewis and Schwartz, 2004; O'Dowd and de Leeuw, 2007; de Leeuw et al., 2011), other factors including sea surface temperature (Mårtensson et al., 2003; Sellegri et al., 2006; Jaeglé et al., 2011; Zábori et al., 2012; Ovadnevaite et al., 2014; Salter et al., 2014, 2015; Schwier et al., 2017; Forestieri et al., 2018; Saliba et al., 2019; Barthel et al., 2019; Christiansen et al., 2019; Hartery et al., 2020; Liu et al., 2021; Zinke et al., 2022; Sellegri et al., 2023), salinity (Mårtensson et al., 2003; Zábori et al., 2012; Ovadnevaite et al., 2014; May et al., 2016; Nilsson et al., 2021; Zinke et al., 2022), and seawater biology and chemistry (O'Dowd et al., 2004; Sellegri et al., 2006; Fuentes et al., 2010; Wang et al., 2015; McCoy et al., 2015a; Schwier et al., 2017; Burrows et al., 2018; Forestieri et al., 2018; Saliba et al., 2019; Christiansen et al., 2019; Sellegri et al., 2023) have also been shown to influence production. Conflicting and sometimes contradictory results for the magnitude and even sign of the impact of each of these variables has been observed in laboratory and field measurements, which has not aided evaluation of the numerous available SSA source parameterizations.

https://doi.org/10.5194/egusphere-2024-2159
Preprint. Discussion started: 25 July 2024

The new Scripps Ocean-Atmosphere Research Simulator (SOARS) wind-wave channel at the Scripps Institution of Oceanography, University of California San Diego was designed to tackle some of these outstanding questions about the production and atmospheric impacts of SSA. This study focuses on first results from the SOARS channel during the CHaracterizing Atmosphere-Ocean parameters in SOARS (CHAOS) mesocosm campaign, conducted for two months in 2022. The overarching goal of CHAOS was to understand and reduce uncertainty in the impact of wind speed on SSA production. Improvements over previous wave channel experiments (Prather et al., 2013; Wang et al., 2015; Sauer et al., 2022) include the ability to modulate wind speed in the wave channel, increasing atmospheric relevance. This study will touch on SSA production in SOARS, but primarily address the role of wind speed in emissions of marine INPs, which has not previously been characterized through controlled experiments.

2 Methods

2.1 Production of Sea Spray Aerosols in SOARS

Measurements described in this study were collected during the CHaracterizing Atmosphere-Ocean parameters in SOARS (CHAOS) study, during August 2022. SSA were produced in the new Scripps Ocean-Atmosphere Research Simulator (SOARS) wind-wave channel at the Scripps Institution of Oceanography (SIO), which is shown schematically in Fig. A1. The SOARS wave channel is 2.4 m wide, 2.4 m tall, and 36 m in length, with a nominal water volume of 103,680 L when filled. This is approximately 9 times the water volume of the glass wave channel described in Sauer et al. (2022), which was used during the preceding Sea Spray Chemistry and Particle Evolution (SeaSCAPE) campaign. Waves are generated with a paddle driven by a TEFC (Totally Enclosed, Fan-Cooled) electric motor, up to a maximum height of 0.9 m. During CHAOS, a repeating wave sequence was used which had 2 breaking waves for every 5 wave crests. SOARS features an enclosed air recirculation system with a split duct design above the wave channel where the wind turbines (fans) are located. There are additional (makeup) fans generating positive pressure to reduce mixing of ambient gas and aerosol into SOARS. Airflow through the makeup fans passes through HEPA and activated charcoal filters prior to entering the air ducts upstream of the main fans. A submerged polycarbonate ramp, or "beach", at the end of the channel dissipates residual wave energy and reduces reflected interference within the breaking wave channel. At low wind speeds, HEPA filters and other user-selectable filters (i.e. activated charcoal) can be included in-line with the air stream in the recirculation vents to remove particles and organic compounds. A "tent" constructed of plastic sheeting was built around the paddle during CHAOS to minimize particle or VOC contamination of the SOARS headspace through paddle motion. The tent was positively pressurized with fans forcing air through MERV 8 and potassium permanganate filters.

Water to fill the SOARS channel is sourced from the Pacific Ocean at the nearby Scripps Pier. Seawater is pumped up at the end of the pier from 1-3 m above the sea floor, roughly filtered with an aluminum screen to remove large detritus, and then passes through a rotating drum filter with a variable mesh filter (18-120 μm) to remove phytoplankton (Jio, 2022). Filtered seawater then travels the length of the pier in a gravity flume. Unlike SeaSCAPE, the water volume required to fill the SOARS channel necessitated using the same plumbing and holding tanks as the nearby Birch Aquarium and other SIO labs instead

https://doi.org/10.5194/egusphere-2024-2159
Preprint. Discussion started: 25 July 2024

of pumping water directly out of the gravity flume and transporting by truck to the channel. At the pier entrance, seawater is passed through several additional coarse filters, fed into a large settling tank, and then filtered through high capacity sand filters prior to being pumped into several large holding tanks (Jio, 2022). Finally, the filtered seawater is pumped or gravity-fed to labs and other facilities. The SOARS channel is filled using either gravity or adjustable-speed water pumps (typically ∼90 gal min^{-1}) and optionally passed through additional filters and/or UV-sterilized. During CHAOS, seawater was not filtered or UV-sterilized, and the channel was gravity-filled from the seawater holding tanks. Four separate fills of the SOARS channel were conducted during CHAOS: July 6-18, July 19-21, August 1-12, and August 14-26, 2022. Only data from the two fills in August 2022 are presented in this study due to instrument availability and technical difficulties with the new paddle assembly. Water temperature can be controlled between -1.6 and 30 °C, and air temperature between -20 and 30 °C. Neither were held constant during CHAOS, and were instead allowed to vary according to the ambient temperature. The channel contains built-in sensors at several locations for measuring air and water temperature, atmospheric CO_2 concentration, and water salinity and turbidity. Since the entire SOARS channel is indoors, there are 2 optional lighting mechanisms. Six solar tubes centered on the middle 1/3 of the channel can provide up to ∼6 % of ambient light, which penetrates the full depth of the channel. 40,000 W of PAR LEDs can provide supplemental lighting during night or stormy conditions.

The SOARS paddle can be programmed to generate wave packets of variable wavelength and amplitude. During CHAOS, two wave packets were superimposed to form 5 wave crests, of which 2 break; this pattern was repeated for the duration of each sampling period. Prior to each sampling period, the headspace air was filtered at a low wind speed to remove particles. Then the wind turbines were set to generate the desired wind speed, and the paddle started to create waves. Occasionally, the wind turbines were run without the paddle, which can generate SSA at wind speeds higher than ∼ 17 m s^{-1}. The wind turbine RPM set points were calibrated using an air velocity meter (TSI Inc. model 9545-A) installed inside the channel with no waves generated. Wind speeds were measured at 0.6 m above the water surface and extrapolated to a value at 10 m (U_{10}) following Hsu et al. (1994). Whitecap coverage was calculated from still images collected at high resolution for every measured wind speed. For each wave packet amplitude, there is a single wind turbine set point which generates a whitecap fraction representative of open-ocean conditions, based on the relationship described in Monahan and Muircheartaigh (1980). During CHAOS, the wave packet amplitude scale was fixed at 1.3, which yields an open-ocean equivalent whitecap coverage at a wind turbine set point of 1550 rpm, corresponding to an extrapolated U_{10} of 18.5 m s^{-1}. Measurements collected during CHAOS were made at wind turbine speeds of 850, 1200, 1400, 1500, 1600, and 1800 rpm, which correspond to U_{10} of 9.57, 13.84, 16.28, 17.50, 18.72, and 21.16 m s^{-1}, respectively. Measurements made at 1600 rpm (18.72 m s^{-1}) are considered to represent open-ocean breaking wave conditions, through comparison with Monahan and Muircheartaigh (1980). For all other wind speeds measured during CHAOS, the fixed wave amplitude meant the whitecap coverage is not comparable to equilibrium open-ocean conditions and only the relative influence of wind speed alone can be assessed.

2.2 Ice Nucleating Particle Measurements

Ice nucleating particle measurements were conducted at all wind speeds. A Colorado State University (CSU) Continuous Flow Diffusion Chamber (CFDC; Section 2.2.1) was used to capture online measurements at high temporal resolution (∼15 min),

https://doi.org/10.5194/egusphere-2024-2159
Preprint. Discussion started: 25 July 2024

and aerosol filter samples were collected and subsequently analyzed with the CSU Ice Spectrometer (IS; Section 2.2.2) to provide INP temperature spectra down to -30 °C. Chemical pre-treatments of aerosol filter suspensions allowed INPs produced in SOARS to be classified by broad composition (Section 2.2.3), and Atomic Force Microscopy was used to assess INP morphology and phase state (Section 2.2.4). Water samples were collected daily from SOARS, and seawater ice nucleating entity (INE) temperature spectra were also measured using the IS as a complement to the aerosol results (Section 2.2.2). CFDC measurements (Section 2.2.1) presented here exclude the first 15 minutes of each sampling period to allow particle concentrations to reach an approximate steady-state. IS filters (Section 2.2.2) were started ∼15 min into each sampling period for the same reason.

2.2.1 Continuous Flow Diffusion Chamber

Real-time measurements of INP concentration were collected using a CSU Continuous Flow Diffusion Chamber (CFDC), a vertically oriented, ice-thermal diffusion chamber (Rogers, 1988; Rogers et al., 2001; DeMott et al., 2015). The HIAPER (CFDC-1H) version of the CFDC used during CHAOS has been previously described in detail and will only be briefly discussed here (e.g. McCluskey et al., 2018a; Moore, 2020; DeMott et al., 2023; Moore et al., 2024). Prior to entering the top of the CFDC chamber, the sample aerosol stream drawn from SOARS was dried to below the frost point with diffusion driers, then passed through two sequential single-jet impactors (50 % aerodynamic diameter cut size D_{50}=2.4 µm) to remove large aerosols. Within the chamber, particles are first exposed to near steady-state humidity and temperature conditions conducive to the activation of cloud droplets and ice crystals, followed by a water-subsaturated region to evaporate haze and cloud droplets back to aerosol sizes. Ice crystals are then detected optically at the base of the chamber using an optical particle counter (OPC) and distinguished by size from aerosols and any remaining cloud droplets (Barry et al., 2021b). The upper region of the chamber was held under water supersaturated conditions (typically 104 % to 108 %) for this campaign to emphasize the immersion freezing mode of ice nucleation and give comparable results to offline techniques (DeMott et al., 2016, 2017, 2018; Barry et al., 2021b).

The aerosol lamina temperature was held at -25 °C or -30 °C during CHAOS to maximize the instrumental signal-to-noise ratio and accommodate limited sampling durations at each wind speed. Paired measurements of the sample air stream (10 min) and HEPA-filtered air (5 min) were used to quantify instrument noise (DeMott et al., 2017). All measurements presented here have been corrected for CFDC background using adjacent filtered-air periods, as in Moore (2020) and Barry et al. (2021b). This correction is achieved using a Poisson model incorporating the detection rates of INPs during ambient and filtered-air measurements. Confidence intervals on INP concentrations and statistical differences between sample and filtered-air periods are assessed at the same time as the background correction, and follow Krishnamoorthy and Lee (2012). All concentrations are converted to standard conditions to allow for direct comparisons between measurements at varying temperatures (STP; 0 °C and 100 kPa).

Nucleated ice crystals were collected for offline analysis following the OPC at the base of the CFDC chamber and analyzed using Atomic Force Microscopy to ascertain differences in INP morphology and phase state with wind speed (Section 2.2.4).

https://doi.org/10.5194/egusphere-2024-2159
Preprint. Discussion started: 25 July 2024

Ice crystals were collected onto substrates using a single-jet impactor with a 50 % cut-size of 4 µm aerodynamic diameter (McCluskey et al., 2014; Barry et al., 2021b).

2.2.2 Ice Spectrometer Measurements

Aerosols produced in SOARS were collected onto pre-cleaned 0.2 µm pore size, 47 mm diameter track-etched polycarbonate membrane filters (Whatman Nuclepore) in pre-sterilized aluminum inline filter housings (Pall), using the protocols described in Barry et al. (2021a). Sample flow rates were held at ∼5 std lpm (slpm) and the sample stream passed through a silica gel diffusion drier prior to particle collection to prevent saturation/wetting of the filters. Filter collection volumes ranged from 182 to 855 std L, with the higher volumes representing longer sampling durations at lower wind speeds to increase particle mass. Blank filters were collected regularly by installing filters in housings and connecting to the same tubing used for SSA sampling, without airflow. Seawater was sampled from either the rear end of the SOARS channel (beach) or underneath the aerosol sampling manifold, approximately halfway up the water column, using a peristaltic pump and silicone tubing to minimize cell rupture for biological measurements. Filters and seawater were either analyzed immediately or stored frozen (-20 °C) prior to analysis.

Offline measurements of INP and INE immersion freezing temperature spectra were made using the CSU Ice Spectrometer (IS), which has been comprehensively described in its present form elsewhere (Hiranuma et al., 2015; DeMott et al., 2018; Hill et al., 2023). Aerosol filters were re-suspended in 8 mL of 0.1 µm filtered DI water, then 50 µL aliquots of either seawater or aerosol suspensions were dispensed into sterile 96-well PCR trays (Optimum Ultra, Life Science Products). Dilutions of each sample were used to extend the measurement temperature range; these were made in 0.1 µm filtered DI water for aerosol filter suspensions and 0.1 µm filtered artificial seawater (NeoMarine, Brightwell Aquatics) for seawater samples. The trays were then placed into temperature-controlled aluminum blocks inside the IS, and cooled at ∼0.33 °C min^{-1}. Freezing events were detected optically from CCD camera images collected at 1 Hz. A 0.1 µm filtered DI water or artificial seawater negative control was included with each IS measurement and used to correct sample results for INPs present in the water used for resuspension and dilution. INP concentrations in the aerosol suspensions or seawater were calculated following Vali (1971), then converted to concentrations in SOARS headspace air for aerosol filters (reported at STP; 0 °C and 100 kPa). Confidence intervals were derived following Agresti and Coull (1998), and the LOD determined as in Moore et al. (2024). The average background number of INPs from the collected blank filters (4) were used to adjust filter sample concentrations; measurements are not reported if blank-corrected values fell below zero (Moore et al., 2024). Temperature spectra of seawater samples have been adjusted by +2 °C to account for freezing point depression due to salinity.

2.2.3 Chemical Composition of INPs in the Ice Spectrometer

Inferences about INP composition are possible from pre-treatments of aerosol filter suspensions or seawater prior to analysis with the IS. Heat treatments are used to assess the contribution of biological INPs to a total sample population (Hill et al., 2016; Suski et al., 2018), as INPs produced by fungi and bacteria are often proteinaceous (Pummer et al., 2015) and denatured by heating. Aliquots of either re-suspended particles from aerosol filters or seawater were immersed in boiling water for 20 min

https://doi.org/10.5194/egusphere-2024-2159
Preprint. Discussion started: 25 July 2024

before being cooled to room temperature and then analyzed with the IS as normal (Section 2.2.2). The difference between the pre- and post-heat treated sample represents the biological INP contribution. The proportion of refractory, typically mineral, INPs are identified through oxidation experiments that remove organic material (Suski et al., 2018; McCluskey et al., 2018c). Sample aliquots are digested for 20 min with 10 % hydrogen peroxide while immersed in boiling water, with two UVB fluorescent bulbs (Exo Terra) illuminating the samples to generate hydroxyl radicals. After cooling, catalase (MP Biomedicals, PN 100429) is added to remove any excess hydrogen peroxide and prevent significant freezing point depression (Suski et al., 2018). The INP temperature spectrum remaining after oxidation is inferred to be the mineral (or other inorganic) component, and the difference between pre-and post-oxidation spectra corresponds to organic INPs.

2.2.4 Single Particle Atomic Force Microscopy of INPs

INPs collected in the CFDC were deposited onto hydrophobically coated (Rain-X) silicon substrates (Ted Pella, Inc.) and stored in clean Petri dishes inside a laminar flow hood (NuAire, Inc., NU-425-400) at ambient temperature (20-25 °C) and pressure prior to analysis (Lee et al., 2020; Kaluarachchi et al., 2022a, b). Samples collected at four wind speeds (9.57, 16.28, 18.72, and 21.16 m s^{-1}) were analyzed to assess the distribution of physicochemical properties under varied wind stress. A molecular force probe 3D AFM (Asylum Research, Santa Barbara, CA) was used to image individual INPs at ambient temperature (20-25°C) and pressure, as described in prior studies (Ray et al., 2019; Lee et al., 2020). A custom humidity cell was used to control RH between 20 % and 60 %. Prior to AFM measurements at a particular RH, samples were allowed to equilibrate for at least 10 minutes to ensure thermodynamic equilibrium with the surrounding water vapor (Lee et al., 2017, 2020; Madawala et al., 2021). Silicon nitride AFM tips (MikroMasch, model CSC37, tip radius of curvature ∼10 nm, nominal spring constant 0.5-0.9 N m^{-1}) were used for AFM imaging and force spectroscopy measurements (Lee et al., 2017; Madawala et al., 2021). AFM AC (intermittent contact) imaging mode was used to collect 3D height images of individual INPs to determine their morphology, and to quantify their volume-equivalent diameter, as described previously (Ray et al., 2019; Kaluarachchi et al., 2022b). For morphological analysis, approximately 50 individual particles were studied for each sample, with volume-equivalent diameters ranging from 0.05 – 1.0 µm. Particles were classified into six main types: rounded, core-shell, prism-like, rod, aggregate and irregular. Example images of particles at 20 % RH in each category are shown in Fig. A2.

Organic particle phase state was identified for samples at 20 % and 60 % RH, as in previous studies (Lee et al., 2017, 2020). These RH values were selected as benchmarks based on previous phase state studies on sucrose that showed solid-to-semisolid and semisolid-to-liquid phase transitions at ∼20 % and 60 % RH, respectively (Lee et al., 2017; Ray et al., 2019; Madawala et al., 2021). Briefly, AFM force spectroscopy (i.e., force plots), was performed on individual core-shell particles at a particular RH by probing within the shell region of each particle. At least five force plots were collected for each individual particle at both 20 % and 60 % RH, with a maximum force of 20 nN and scan rate of 1 Hz. The viscoelastic response distance (VRD) and relative indentation depth (RID), or ratio of the indentation depth to the particle height, were then quantified, which can be related to the viscosity of the material (Lee et al., 2020; Kaluarachchi et al., 2022a). A previously reported framework based on VRD and RID measurements was then utilized to identify the phase state of each particle at 20 % and 60 % RH (Lee et al.,

https://doi.org/10.5194/egusphere-2024-2159
Preprint. Discussion started: 25 July 2024

2017). A total of 5, 19, 12, and 13 individual core-shell particles were studied for the 9.57, 16.28, 18.72, and 21.16 m s^{-1} wind speed conditions, respectively (Table A1).

Since the total number of individual particles that can be realistically studied with AFM is somewhat limited, a probability distribution analysis to assess the statistical significance of the AFM results was employed (Cappa et al., 2021, 2022; Kaluarachchi et al., 2022b). Briefly, the probability distribution curves associated with the likelihood of sampling one of the six particle morphology types, or one of the three phase states, were generated using a Markov chain Monte Carlo method for a "true" population of 10,000 particles. The resulting distributions were fit with Gaussians to provide standard deviation estimates for both morphology and phase state measurements.

2.3 Aerosol Size Distribution Measurements

Several dedicated instruments were used to measure aerosol size distributions during CHAOS, using different aerosol inlet configurations. All aerosol streams were dried with silica gel diffusion driers prior to measurement to below the efflorescence relative humidity of sea salt, ~45-48 % (Tang et al., 1997). The first set of measurements used in this study consist of a TSI Scanning Mobility Particle Sizer (TSI, SMPS 3936) for aerosols in the range 14-750 nm and a TSI Aerodynamic Particle Sizer (TSI, APS 3321) for particles between 0.5-20 µm. The SMPS and APS sampled from a 3/8 inch diameter stainless steel inlet that entered the side of the SOARS channel and then turned 90° to face into the air flow. It was located approximately 0.6 m above the water surface and angled roughly 45° below horizontal, towards the water's surface. The INP filter measurements were made with a similar inlet located 2-3 m further down the channel, but oriented parallel to the water's surface. A second set of aerosol measurements were collected with a Scanning Electrical Mobility Analyzer (BMI, SEMS model 2002) between 10 and 1340 nm (mobility diameter) and another Aerodynamic Particle Sizer (TSI, APS model 3321), both of which sampled behind a 2.5 µm cyclone. The SEMS and APS data were merged at 650 nm after converting the APS from aerodynamic to mobility diameter assuming a particle density of 2.0 g cm^{-1}. The SEMS and APS sampled from a shared aerosol manifold with the CFDC, which had a vertically oriented 1/2 inch diameter stainless steel inlet that entered from the top of the SOARS channel and sampled ~0.6 m above the water surface. Theoretical particle transmission efficiency calculations were performed for both sets of inlets (INP filter/SMPS + APS and CFDC/SEMS + APS) and are shown in Fig. A3 as a function of the SOARS fan speed. These calculations were performed in aerodynamic diameter with a particle density ρ=1 and later corrected for expected particle density, water uptake, and shape factor following Tang et al. (1997) and Zieger et al. (2017). Significant vibrations and vertical movement of the INP filter and SMPS + APS sampling inlets were observed at higher wind speeds, with unknown effects on particle line losses that are not accounted for in these theoretical calculations.

These particle measurements were primarily used to normalize the INP concentrations, as described in Section 3.1. Particle surface area and volume distributions were calculated for each number distribution assuming particle sphericity, as were number concentrations of particles larger than 500 nm dry diameter (n500). Due to the differences in expected aerosol transmission (Fig. A3) between the horizontally and vertically oriented inlets, the SMPS + APS data was used to normalize the INP filter results. The SEMS + APS observations were intended to correct the CFDC data, however, SEMS data was only available for the second half of August. So instead, data from the OPC at the base of the CFDC chamber, which is limited to particles larger

https://doi.org/10.5194/egusphere-2024-2159
Preprint. Discussion started: 25 July 2024

than ∼300 nm, was used to provide aerosol concentrations to normalize the CFDC INP measurements. Correction factors for total particle number, n500, surface area, and volume concentrations were derived for the CFDC OPC based on the available SEMS data (Fig. A4) and applied to the OPC observations shown here.

CFDC operation requires the incoming air stream to be dried to below the frost point at the given measurement temperature (typically -25 °C or -30 °C), so aerosols enter the CFDC at dry sizes. However, particles will deliquesce, and some will activate into cloud droplets under the water supersaturated conditions present in the top section of the CFDC chamber. Any particles not activated into ice crystals will evaporate in the water-subsaturated region at the bottom of the chamber (Section 2.2.1), which is held at ice saturation. Following Murphy and Koop (2005), the saturation vapor pressures with respect to ice and water were calculated during each period based on the measurement temperature, as well as the resulting RH. Dry particle sizes were estimated assuming spherical, sea salt particles with a hygroscopic growth factor (HGF) of 1.7 for the 70-75 % RH range calculated (Zieger et al., 2017). The CFDC OPC was calibrated against polystyrene latex spheres (PSLs) and glass beads of known sizes and refractive indices, and size distributions calculated assuming a refractive index of n=1.5 for sea salt (Tang et al., 1997).

3 Results and Discussion

3.1 SSA and INP production at Varying Wind Speeds

Measurements of both SSA and INPs were made at six U_{10} wind speed equivalents (9.57, 13.84, 16.28, 17.50, 18.72, and 21.16 m s^{-1}) during CHAOS. Normalized histograms of integrated particle number, number >500 nm diameter (n500), surface area, and volume concentrations are shown in Fig. 1 for all measured wind speeds from the corrected CFDC OPC measurements, and example size distributions from the SEMS + APS and SMPS + APS in Fig. A5 (Sec. 2.3). As expected from numerous previous measurements (e.g. Lewis and Schwartz, 2004; O'Dowd and de Leeuw, 2007; de Leeuw et al., 2011), particle concentrations generally increased with wind speed in the SOARS channel. Large variability in each aerosol metric was observed at all wind speeds (Fig. A5), with a clear increase in aerosol concentration between the 16.28 and 17.50 m s^{-1} wind speeds. This variability occurred for measurements collected both days or weeks apart and on the same day, if wind speeds were repeated, and the source is unknown (see Fig. A5). A previous study of wind profiles in a wind-wave tank (Vollestad and Jensen, 2021) found that while the horizontal wind speed displayed the expected, approximately logarithmic profile, secondary flows due to the confined channel were found to impact the observed vertical velocity structure. Modification of the near-surface wind and turbulence due to the presence of waves has been observed in wind-wave tanks (Zavadsky and Shemer, 2012; Villefer et al., 2021) and in models (Chen et al., 2019), and varies with the fetch (Lamont-Smith and Waseda, 2008), as well as the presence of swell in addition to wind-waves (Villefer et al., 2021). Variation in secondary flow structure is a possible explanation for some of the variability seen in particle concentrations at the same nominal wind speed during CHAOS.

The maximum observed values for particle number, surface area, and volume were much larger during CHAOS than Southern Ocean values (Moore et al., 2022), by factors of ∼50, ∼45, and ∼7, respectively. At least some of these differences are likely a result of the differences in time scale and fetch, with open ocean measurements closer to steady state, and integrated

https://doi.org/10.5194/egusphere-2024-2159
Preprint. Discussion started: 25 July 2024

over a larger area with potentially more variability. Additionally, the SOARS channel is a closed system where horizontal and vertical SSA fluxes are suppressed, allowing particle concentrations to build until losses are equal to emissions. Size distribution measurements (Fig. A5) suggest the size distribution shape and mode size is similar across wind speeds in SOARS, but with larger variability in number concentration at higher wind speeds, particularly in the accumulation mode. At wind speeds below 18.5 m s^{-1}, the fixed 1.3 amplitude-scaled waves generated by the SOARS paddle led to higher whitecap coverages than would be anticipated in the open ocean for equilibrium conditions, and for the highest, 21.16 m s^{-1}, whitecap coverage was lower than open ocean values (Monahan and Muircheartaigh, 1980). This likely led to an overestimation of particle production at low wind speeds and underestimation at the highest. Additional tests are currently underway to study particle production when the wave amplitude is varied along with the wind speed to match open ocean whitecap fractions, which may reduce some of the large observed variability in particle production at some wind speeds during CHAOS.

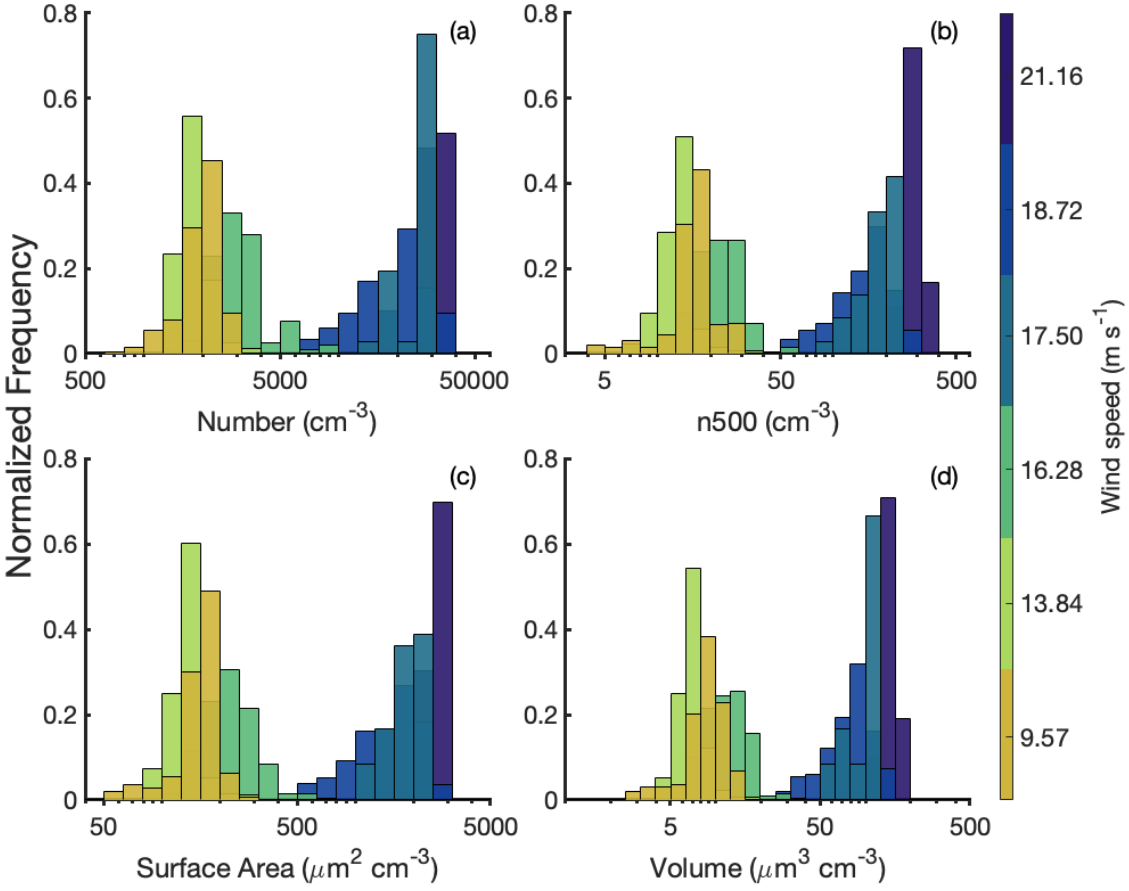

Figure 1. Normalized frequency distributions of particle (a) number, (b) number >500 nm diameter (n500), (c) surface area, and (d) volume concentrations at each measured wind speed during CHAOS.

https://doi.org/10.5194/egusphere-2024-2159
Preprint. Discussion started: 25 July 2024

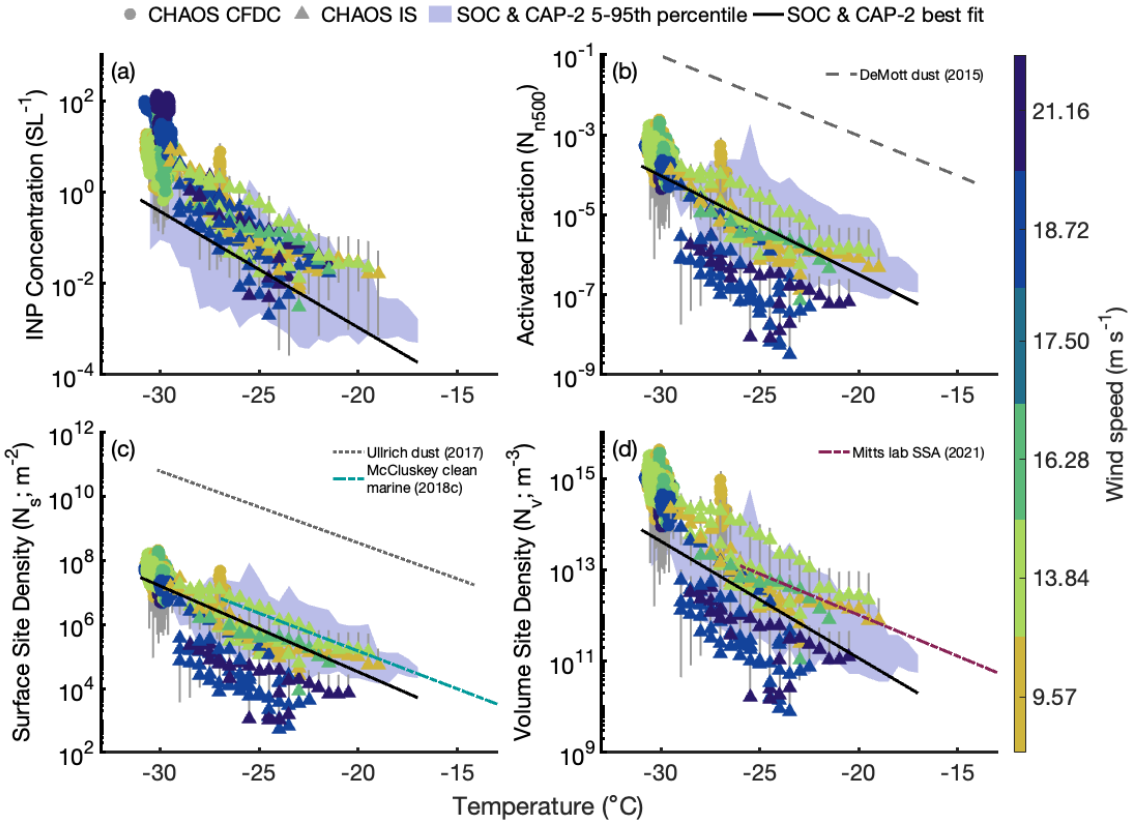

Figure 2. INP (a) number concentration, (b) normalized by n500 (N_{n500}), (c) normalized by aerosol surface area (N_s) and (d) normalized by aerosol volume (N_v) temperature spectra during CHAOS. CFDC measurements are indicated by circles and IS filter observations by triangles; both are colored by the wind speed during each measurement period. The purple shading in each panel indicates the 5th-95th percentile of values observed in the marine boundary layer during SOCRATES and CAPRICORN-2 (Moore et al., 2024), and solid black lines are the best-fit lines for each variable from these campaigns. In (b), the grey dashed line shows the DeMott et al. (2015) parameterization for dust based on n500, using the median n500 value measured during 18.72 m s^{-1} wind speed periods. In (c), the grey dotted line indicates the Ullrich et al. (2017) parameterization for dust N_s, and the blue dot-dash line shows the N_s parameterization from McCluskey et al. (2018c) for North Atlantic clean marine air. The dashed magenta line in (d) indicates the Mitts et al. (2021) lab-based parameterization for marine N_v.

A summary of the INP results from CHAOS, along with relevant model parameterizations, are displayed in Fig. 2, which shows INP measurements from the CFDC (Section 2.2.1) and IS filters (Section 2.2.2) as a function of temperature. Similar observations made in the Southern Ocean marine boundary layer during the Southern Ocean Cloud Radiation Aerosol Transport
335 Experimental Study (SOCRATES, hereafter SOC) aircraft campaign and the second Clouds, Aerosols, Precipitation, Radiation and atmospherIc Composition Over the southeRN ocean (CAPRICORN-2, hereafter CAP-2) ship campaign are shown in each panel in the light purple shading (Moore et al., 2024). Figure 2a shows measured INP concentrations, while the other panels show different normalizations commonly used in models (Fig. 2b-c) or suggested for marine INPs (Fig. 2d). Figure 2b displays

https://doi.org/10.5194/egusphere-2024-2159
Preprint. Discussion started: 25 July 2024

INP concentrations normalized by n500 (N_{n500}), which has been used previously for dust (DeMott et al., 2015) and biological INPs (Tobo et al., 2013) due to observed relationships with supermicron aerosol. Figure 2c is normalized by aerosol surface area, which has been widely used for multiple INP types, including marine INPs (Niemand et al., 2012; Ullrich et al., 2017; McCluskey et al., 2018c). Normalization by aerosol volume (Fig. 2d) was suggested by Mitts et al. (2021) for marine INPs on the basis of laboratory experiments, but measurements from the Southern Ocean (Moore et al., 2024) did not support a similar relationship for ambient data, and nor do these measurements from CHAOS.

INP concentrations and normalized values vary in their consistency with CAP-2 and SOC measurements (Fig. 2), which themselves agreed well with previous observations from the Southern Ocean and mid-latitude North Atlantic (McCluskey et al., 2018a; Schmale et al., 2019; Tatzelt et al., 2022; Moore et al., 2024). In general, CHAOS measurements at wind speeds <17 m s^{-1} agree with those from SOC and CAP-2 and those at higher wind speeds do not, although there are some differences between CFDC and IS observations that will be discussed more below. INP concentrations during CHAOS were on the high end (above the 50th percentile) of Southern Ocean values, and CFDC (≤-27 °C) measurements at wind speeds above 17 m s^{-1} are above the 95th percentile of CAP-2 and SOC values by about an order of magnitude. As anticipated, the DeMott et al. (2015) n500-based parameterization (Fig. 2b) and Ullrich et al. (2017) N_s parameterization (Fig. 2c) for dust INPs overestimate CHAOS values by several orders of magnitude. N_{n500} and N_s measured by the CFDC during CHAOS overlap with Southern Ocean observations, though are biased high (Fig. 2b-c). IS N_{n500} and N_s values for wind speeds <17 m s^{-1} are within the 5th-95th percentile of CAP-2 and SOC values, while those at high wind speeds are almost entirely below the 5th percentile. Interestingly, the agreement for N_v is better overall, although CFDC measurements are all above the 50th percentile and extend above the CAP-2 and SOC 95th percentile, while IS measurements at higher wind speeds fall below the 5th percentile (Fig. 2d). Similarly to the CAP-2 results (Moore et al., 2024), the Mitts et al. (2021) N_v parameterization has a lower slope than the CHAOS dataset, and is near the upper bound of measured values at all temperatures. Variable agreement among N_{n500}, N_s, and N_v suggests a different shape to the particle size distribution in the SOARS channel than the Southern Ocean MBL, since all of the aerosol concentrations are enhanced in SOARS relative to ambient measurements (Fig. 1), but only N_v has a similar range as ambient observations. This is supported by example size distributions from CHAOS, which show enhancements in aerosol concentrations between 0.1 - 1 μm relative to CAP-2 distributions, with the discrepancy increasing with wind speed (Fig. A5).

CFDC INP concentrations (circles in Fig. 2, ≤-27 °C) generally increase with wind speed, while variability is reduced following normalization by aerosol concentrations, as expected if INPs are emitted proportionally to SSA. The reduction in spread after normalization is shown even more clearly in the time series of CFDC data presented in Fig. A6. However, it is also clear from Fig. A6 that on some days, INP concentrations were the same up to a wind speed threshold of ∼17 m s^{-1} (8/8/22, 8/17-8/19/22). Other days did not sample enough wind speeds to assess this variation. This agrees with what was observed for SSA concentrations in Fig. 1, which showed a distinct increase in aerosol concentrations between the 16.28 and 17.50 m s^{-1} wind speeds.

On the other hand, INP concentrations measured from the aerosol filters (triangles in Fig. 2, ≥-28 °C) did not have a clear relationship with wind speed. This difference may be due to the different averaging times of the CFDC (∼5 minutes) versus the IS filters (2-3 hr), differences in inlet orientations or locations (Sec. 2.3), or differences in the aerosol sampled.

https://doi.org/10.5194/egusphere-2024-2159
Preprint. Discussion started: 25 July 2024

The CFDC sampled ~2 m upstream of the filters, with a vertically oriented inlet, whereas the IS filters used a horizontal inlet facing into the wind. Despite the anticipated enhancements in particle transmission ~1 μm for the IS filter inlet at higher wind speeds and otherwise similar efficiencies to the CFDC inlet (Fig. A3), the consistently higher concentrations measured by the CFDC at the same wind speed suggest particle losses in the IS filter inlet may not be accurately captured by these theoretical calculations. Future studies should make both online and offline measurements on the same or more similar inlets to reduce these uncertainties. The IS and CFDC are also largely measuring INPs at different temperatures, with the CFDC primarily targeting INPs active ~ -30 °C and the IS sensitive to INPs at warmer temperatures. Temperature-dependent differences in INP composition may also be driving the observed discrepancy between the IS and CFDC results, especially if emission of different types has contrasting dependencies on wind speed.

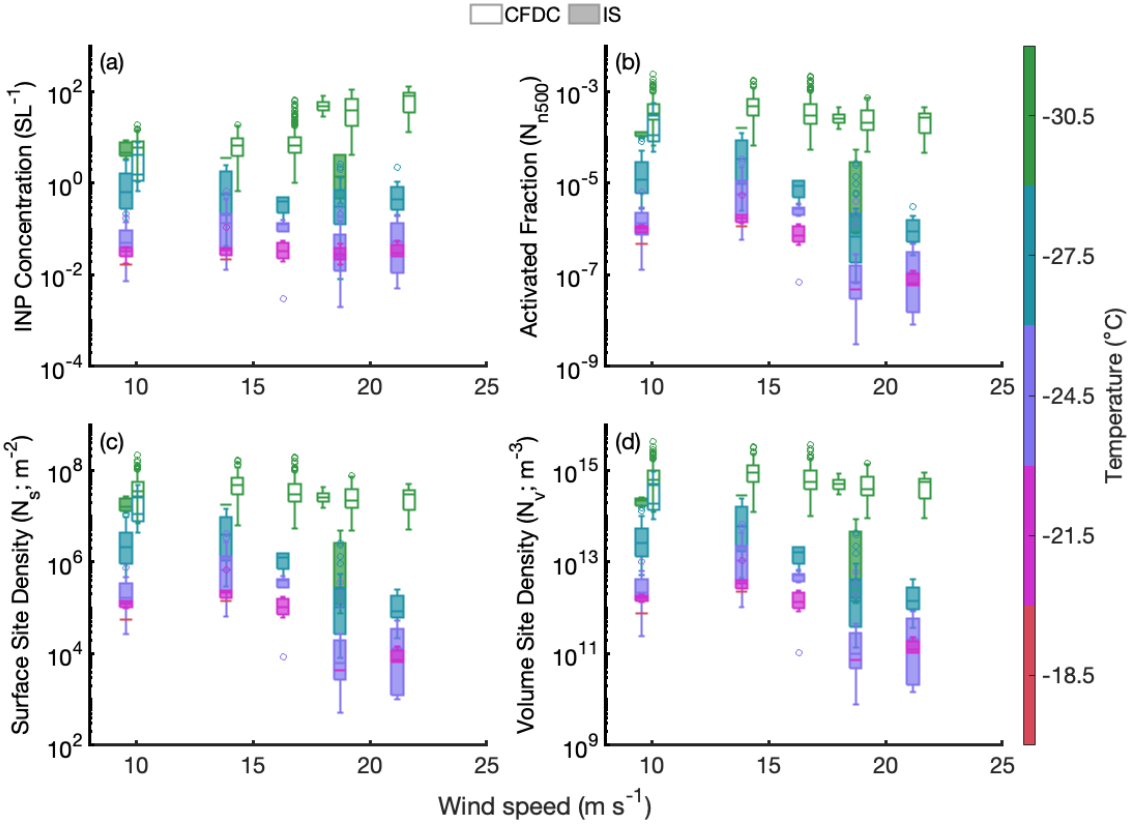

Figure 3. Box plots of observed (a) INP concentration, (b) N_{n500}, (c) N_s and (d) N_v as a function of wind speed during CHAOS. Observations are separated into 3 °C temperature bins (indicated by color), with CFDC measurements shown as open boxes and IS filter data as shaded boxes. CFDC data are offset to the right by +0.5 m s^{-1} for clarity.

Normalized INP concentrations for both instruments generally decreased with increasing wind speed, especially above ~17 m s^{-1}, although decreases were more modest for the CFDC than the IS. This can be seen more clearly in Fig. 3, which displays the same data as Fig. 2 as a function of wind speed in 3 °C temperature bins, with CFDC and IS filter ranges

https://doi.org/10.5194/egusphere-2024-2159
Preprint. Discussion started: 25 July 2024

indicated by box plots. Also clear in Fig. 3 is the large inter-sample variability observed during CHAOS for measurements collected at similar wind speeds and temperatures. INP concentrations in the Southern Ocean MBL were found to increase with wind speed, and to retain the same wind speed dependence after normalization by aerosol number, surface area, and volume (Moore et al., 2024). Even if only considering the CFDC observations, normalized INP concentrations have a small but negative relationship with wind speed during CHAOS. One possible explanation is that loss mechanisms such as dry and wet deposition have lower rates in SOARS, where aerosol was sampled from 0.6 m above the water surface, compared to the ambient marine boundary layer, where measurements were collected from 18.4 m above sea level on the ship and ∼150 m on the aircraft during CAP-2. This would alter the particle size distributions in SOARS, especially at larger sizes where loss rates are higher. As discussed earlier, higher concentrations were seen in the accumulation mode during CHAOS than CAP-2 (Fig. A5). Unfortunately, losses at larger sizes are hard to assess with the available size distribution measurements since the SEMS + APS sampled behind a 2.5 µm cyclone and the SMPS + APS had an inlet similar to the IS (Sec. 2.3) and thus likely also experienced additional losses not accounted for in the theoretical calculations. Overall, the results from CHAOS may be more representative of interfacial fluxes rather than marine boundary layer or cloud-base values. As previously discussed in relation to measured particle concentrations, the fixed 1.3 amplitude scaling for wave height used during CHAOS may also be obscuring the true INP-wind speed relationships, which requires further measurements with co-varying wave amplitude and wind speed to resolve. Seawater INE concentrations were relatively stable throughout CHAOS (Fig. A7) and agree well with previous measurements from the Scripps Pier, as well as the North Indian Ocean (Beall et al., 2022) and mid-Atlantic (Gong et al., 2020), and are higher than observations from the Southern Ocean (McCluskey et al., 2018a) or Barents Sea (Hartmann et al., 2021) by 1-2 orders of magnitude. The INE stability across multiple fills of the SOARS channel and over time with the same water indicates the observed INP-wind speed relationships were driven by wind-wave interactions rather than biological activity in this experiment.

3.2 INP Composition and Phase State Changes under Increasing Wind Speeds

The fractional composition of INPs (Section 2.2.3) as a function of wind speed is shown in Fig. 4 for three temperature ranges: -19 to -23 °C, -23 to -26 °C, and -26 to -29 °C. Composition data is only reported when the treated and un-treated sample were different at the 95 % confidence level, and the fraction of data not meeting this criteria are shown in Fig. A8 as a function of temperature. The generally low fractions of heat treated spectra that significantly differed from the base spectra (green dots in Fig. 4c,f,i) indicate the collected INPs were largely unaffected by heat treatments, although consistently high biological fractions (∼1) were observed at temperatures >-23 °C and wind speeds below 15 m s^{-1} (Fig. 4a-c). Low wind speeds (<∼13 m s^{-1}) may favor enrichment of biological INPs in the sea surface microlayer (Wilson et al., 2015; Engel et al., 2017; Irish et al., 2017; Ickes et al., 2020; Hill et al., 2023), which is consistent with this result. On several days, especially at the end of the second water fill (8/16/22-8/19/22), heat treatments led to increased INP concentrations over the untreated filters at temperatures of -23 to -26 °C, which are shown as biological fractions >1 in Fig. 4d-e, especially at the highest wind speeds. This observation is uncommon but was observed by McCluskey et al. (2018b) during a laboratory-simulated phytoplankton bloom grown in a Marine Aerosol Reference Tank (MART; Stokes et al., 2013). It was suggested to be a result of lysis of

https://doi.org/10.5194/egusphere-2024-2159
Preprint. Discussion started: 25 July 2024

microbial cells upon heating, releasing IN-active material, or the dissolution and redistribution of organic material between particles, leading to a net increase in the number of particles with IN-active organic material. This contrasts with the consistent decrease after heating also presented in McCluskey et al. (2018b) for a phytoplankton bloom grown in the SIO glass channel during the IMPACTS (Investigation into Marine Particle Chemistry and Transfer Science) campaign (Wang et al., 2015), where larger proportions of biological INPs were inferred to be released in response to increased seawater biological activity.

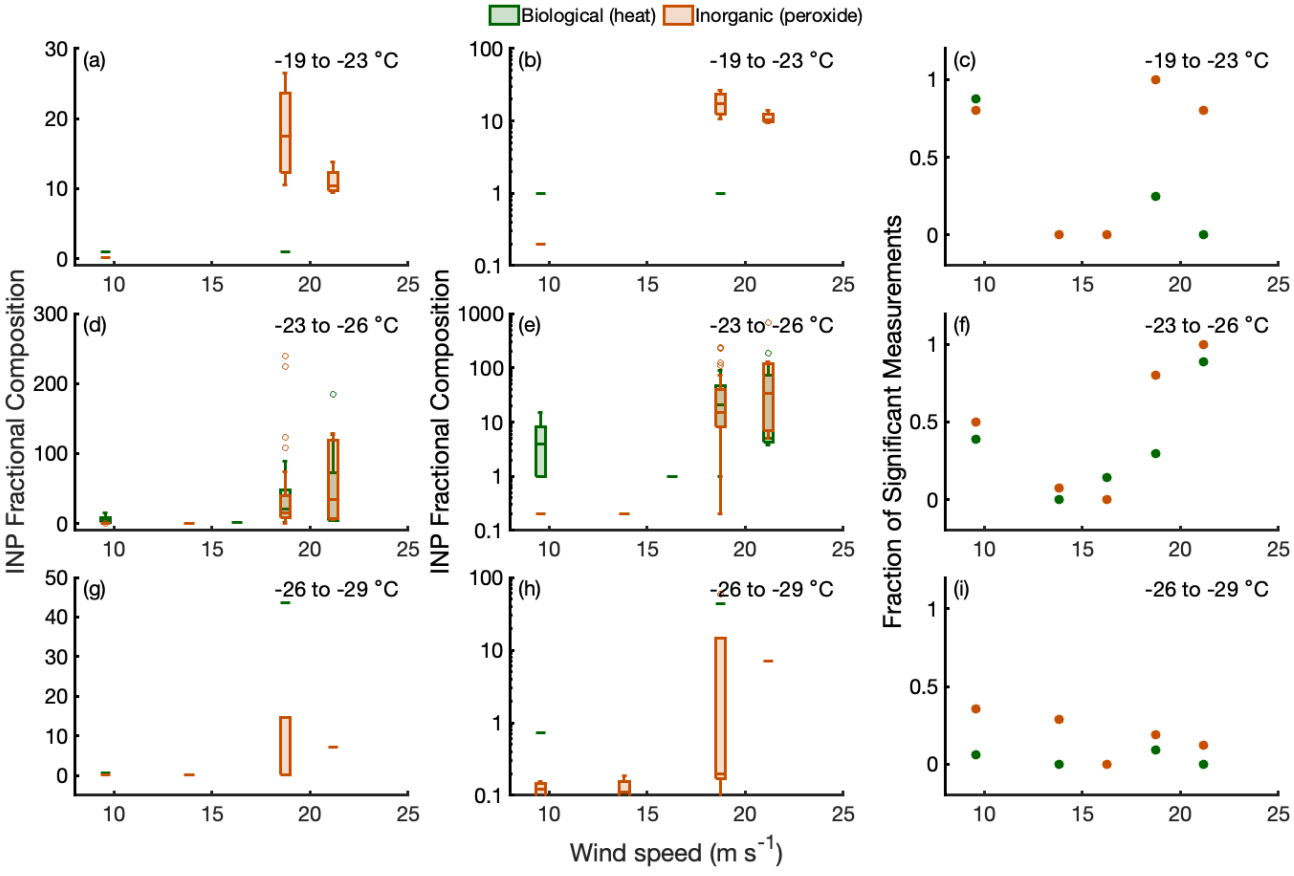

Figure 4. Box plots of biological (green) and inorganic (orange) INP fractional composition as a function of wind speed for IS filter measurements at (a) -19 to -23 °C, (d) -23 to -26 °C, and (g) -26 to -29 °C. Panels (b), (e), and (h) are identical to (a), (d), and (g), respectively, except with a log y-axis so smaller values are visible; zero values are plotted at a fixed value of 0.2 on the log axes. Only treatments that differ from the base spectra at the 95% confidence level are included in (a-b), (d-e), and (g-h). Panels (c), (f), and (i) indicate the fraction of measurements meeting this criteria as a function of wind speed and at temperatures of -19 to -23 °C (c), -23 to -26 °C (f) and -26 to -29 °C (i).

At low wind speeds (<15 m s^{-1}) and below -23°C, heat-stable organic INPs (low biological and low inorganic fractional composition) were the dominant INP type, corresponding to the DOC-INP type described in McCluskey et al. (2018b). This is in accordance with a number of laboratory (McCluskey et al., 2018b) and field (Rosinski et al., 1987; Wilson et al., 2015;

https://doi.org/10.5194/egusphere-2024-2159
Preprint. Discussion started: 25 July 2024

Ladino et al., 2016; Alpert et al., 2022) measurements, although other studies have inferred the dominance of proteinaceous or heat-labile material (Knopf et al., 2011; Wang et al., 2015; Irish et al., 2017). By contrast, at higher wind speeds, inorganic or refractory INPs were the dominant type observed at all temperatures. At wind speeds >15 m s^{-1}, nearly all peroxide-treated filter samples had higher INP concentrations than the untreated samples (inorganic fractional composition >1 in Fig. 4a-b, d-e, g-h), and many of these corresponded to the heat-treated samples with enhanced INP concentrations described above. All of the samples with enhanced concentrations following peroxide digestion had a characteristic shape to their temperature spectra, an example of which is shown in Fig. A9. In contrast to the typical log-linear marine INP spectra (DeMott et al., 2016), dramatic increases are seen in peroxide-treated results at warm temperatures, which flatten out ∼-23 °C and meet or approach the untreated spectra around -27 °C. This is reminiscent of INP temperature spectra identified as biological (Hill et al., 2016; Suski et al., 2018), which have large warm temperature INP populations which are reduced to log-linear spectra following heating and/or peroxide digestion, only inverted. An increase in INP concentration after peroxide digestion has not been reported before for marine INPs, but is hypothesized to be the result of enhanced release of large particles at high wind speeds in SOARS, which may contain multiple INPs. The production of spume droplets through the tearing of wave crests, which produces particles predominantly >10 µm and is increasingly active for wind speeds exceeding ∼9 m s^{-1} (Monahan et al., 1986; Sofiev et al., 2011), is the most likely mechanism consistent with the observed wind speed dependence. The atmospheric lifetime of such particles is very short, which may explain why this has not been observed in ambient measurements or laboratory studies with low wind speeds. Organic material in seawater, including carbohydrates, lipids, and proteins, are well known to self-assemble into microgels which can range in size from <10 nm (single macromolecule) to µm-sized colloidal gels (Chin et al., 1998; Verdugo, 2012). INPs could be trapped in this gel matrix, emitted as large spume drops, and then released following the breakdown of the organic material during peroxide digestion. If so, the composition of the INPs themselves cannot be inferred from these results, since they could be either inorganic contaminants (dust) which are stable against peroxide digestion, or heat-stable organics which the 20-min digestion used here is not long enough to both release from their gel matrix and break down.

Additional information about the composition of INPs produced in SOARS was provided by AFM analysis of submicron ice crystal residuals collected in the CFDC (Section 2.2.4). Six particle categories were identified based on 3D height images of particles collected at 4 wind speeds (9.57, 16.28, 18.72, and 21.16 m s^{-1}): rounded, core-shell, prism-like, rod, aggregate and irregular (Fig. A2). These are similar to the categories identified for ice crystal residuals during SeaSCAPE (DeMott et al., 2023), except rod and irregular particles were not identified during SeaSCAPE. Some of the particles in the rod and irregular classes are morphologically similar to known contaminants from the SOARS channel itself, and these particle classes will not be further discussed here. Prism-like particles did not display a clear relationship with wind speed (Fig. 5). Rounded particles had relatively higher abundances at low wind speeds (<17 m s^{-1}), while core-shell particles increased in relative contribution with increasing wind speeds. Similar collections of SSA produced during CHAOS had identical relationships between relative contributions of core-shell and rounded particles with wind speed as the ice crystal residuals, suggesting the INPs are subsets of all the observed SSA particle morphologies (Madawala et al., 2024, in review). The SSA particles collected were also analyzed for elemental composition by scanning electron microscopy coupled with energy dispersive X-ray spectroscopy (SEM-EDX) as

https://doi.org/10.5194/egusphere-2024-2159
Preprint. Discussion started: 25 July 2024

in Ault et al. (2013) and functional group characterization using atomic force microscopy-Photothermal Infrared spectroscopy (AFM-PTIR) following Or et al. (2018). SEM-EDX indicated rounded SSA particles were organic carbon throughout, while core-shell particles had a cubic NaCl core and organic shell. Rounded particles had more diverse organic functional groups (fatty acids, complex sugars and in some cases traces of sulfates and carbonates), and their composition was similar at both 9.57 and 18.72 m s^{-1}. Core-shell particles were dominated by aliphatic compounds at 9.57 m s^{-1}, with the addition of oxygenated organics at 18.72 m s^{-1} (Madawala et al., 2024, in review).

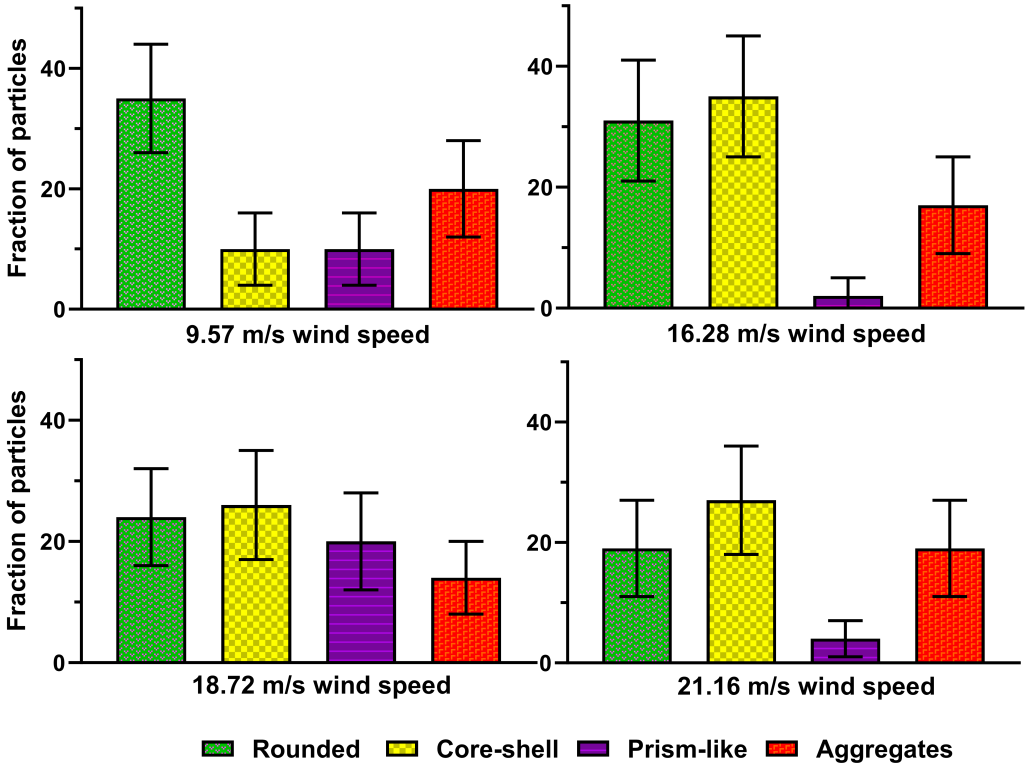

Figure 5. Percentage of particles from each morphological category observed during CHAOS at four of the measured wind speeds (9.57, 16.28, 18.72, and 21.16 m s^{-1}). For each sample, the individual particles (N = 50 for each sample) characterized were in the volume-equivalent diameter range of 0.05 – 1.0 µm.

Viscoelastic response distance (VRD), which is related to the viscosity of the material (Lee et al., 2020; Kaluarachchi et al., 2022a), as well as particle phase state (Lee et al., 2017, 2020) was quantified for core-shell ice crystal residuals at 20 % and 60 % RH (Table A1). As anticipated due to the hygroscopicity of SSA, the fraction of semisolid shells increased between 20

https://doi.org/10.5194/egusphere-2024-2159
Preprint. Discussion started: 25 July 2024

and 60 % RH at all wind speeds. Below 17 m s^{-1}, the shell region of core-shell particles was predominantly solid at 20 % RH, while at higher wind speeds, shells were more often semisolid even at low RH. VRD measurements were only possible on semisolid shells, and were similar at both 20 % and 60 % RH for a given wind speed, but were higher for wind speeds >17 m s^{-1}. The increased abundance of semisolid shells with higher VRD is consistent with lower viscosity and the presence of more oxygenated chemical species in the shell region of core shell particles at higher wind speeds.

4 Conclusions

Initial results from the CHAOS campaign were presented here, which focused on the role of wind speed in the production of SSA and INPs, using the new SOARS wind-wave channel at the Scripps Institution of Oceanography. As expected from numerous field and laboratory measurements, SSA concentrations increased with increasing wind speed (Fig. 1). Enhanced particle concentrations were observed relative to Southern Ocean MBL measurements in a similar wind speed range (Moore et al., 2022) by maximum factors of ∼50, ∼45, and ∼7 for particle number, surface area, and volume, respectively. INP concentrations were broadly consistent with previous measurements from the Southern Ocean (McCluskey et al., 2018a; Schmale et al., 2019; Moore et al., 2024) and North Atlantic (McCluskey et al., 2018c), although SOARS concentrations were biased high and normalized concentrations biased low relative to ambient results (Fig. 2). This is likely related to the low sampling height over the water surface during CHAOS (0.6 m), which may capture more large particles than are typically sampled during ship-board or coastal campaigns where aerosol inlets may be 20+ m above sea level and/or offset from the shore. As a result, measurements from CHAOS likely represent interfacial values and may not be directly comparable to MBL or cloud-base measurements.

INP concentrations also generally increased with wind speed, especially for the CFDC measurements, as was observed in the Southern Ocean MBL (Moore et al., 2024). However, normalized INP concentrations decreased with increasing wind speeds during CHAOS, while the opposite relationship was observed in Moore et al. (2024) for the Southern Ocean (Fig. 2, Fig. 3). In addition to the low sampling inlet height and consequently lower particle losses, the fixed 1.3 amplitude scaling for wave height used during CHAOS may help explain this discrepancy. Further measurements where wind speed and wave amplitude are both varied to produce whitecap fractions representative of open ocean conditions (Monahan and Muircheartaigh, 1980) are required to separate these mechanisms. Additionally, the large spread and highly variable particle concentrations observed for both SSA and INPs during CHAOS complicated analysis and should be addressed through detailed estimates of particle losses within the SOARS channel and inlets and more systematic sampling of wind speeds than was possible during CHAOS due to time constraints. Seawater INE concentrations during CHAOS were stable and consistent with previous measurements at the SIO pier and in other regions (McCluskey et al., 2018a; Gong et al., 2020; Hartmann et al., 2021; Beall et al., 2022), indicating changes in atmospheric INPs during CHAOS were driven by wind speed and wave-breaking mechanics rather than variations in seawater chemistry or biology (Fig. A7).

Heat-stable organic INPs were the dominant composition at wind speeds below 15 m s^{-1} (Fig. 4, Fig. A8), which corresponds to the DOC-type marine INP described in McCluskey et al. (2018b). A number of field measurements have also identified

https://doi.org/10.5194/egusphere-2024-2159
Preprint. Discussion started: 25 July 2024

similar small, heat-stable marine INPs (Rosinski et al., 1987; Wilson et al., 2015; Ladino et al., 2016; Alpert et al., 2022), although a second category of larger and protinaceous (heat-labile) marine INPs has also been observed in both field and laboratory measurements (Knopf et al., 2011; Wang et al., 2015; Irish et al., 2017; McCluskey et al., 2018b). At high wind speeds, peroxide-treated filter samples almost uniformly had higher INP concentrations than untreated samples (Fig. 4, Fig. A9), which has not been previously seen for marine INPs. We hypothesize that spume droplet production at higher wind speeds, coupled with the low height of the SOARS sampling inlet, may have allowed for the sampling of larger, aggregate particles containing multiple INPs, which were broken up through peroxide digestion. The composition of INPs emitted in such gels is unknown, since results from CHAOS are consistent with dust or other inorganic contaminants that are unaffected by peroxide digestion, or heat stable organics which are only released from the larger particle and not broken down due to the 20-min digestions performed here. The very short atmospheric lifetime of large (>10 μm) spume droplets may explain why this has not been seen in ambient measurements or laboratory experiments without wind (Wang et al., 2015; McCluskey et al., 2018b). Entrapment of INEs in gels may also play a role in their low number concentrations in seawater (McCluskey et al., 2018a; Gong et al., 2020; Hartmann et al., 2021; Beall et al., 2022) compared to terrestrial sources such as soil or mineral dust, fungi, and permafrost (O'Sullivan et al., 2014; Fröhlich-Nowoisky et al., 2015; Hill et al., 2016; Kanji et al., 2017; Barry et al., 2023) due to both reduced emissions of large particles and enhanced oceanic deposition through marine snow formation or other processes.

AFM 3D height images of collected ice crystal residuals were used to identify 6 dominant particle morphologies, which were similar to residual classifications during SeaSCAPE (DeMott et al., 2023). Rounded particles were the most abundant morphology at wind speeds <17 m s^{-1}, and core-shell particles dominated at higher wind speeds (Fig. 5). The abundance of core-shell particles with semisolid shells increased with wind speed, while the viscosity of the shells simultaneously decreased. This is consistent with an increasing contribution of oxygenated chemical species in the shells, which was also noted as an outcome of heterogeneous aging of INPs during SeaSCAPE (DeMott et al., 2023). It is possible the decreased viscosity and more complex chemical composition at high wind speeds is related to the enhancement in INP concentration following peroxide digestions through increased water solubility of the shells, as was observed during SeaSCAPE for aged SSA (Kaluarachchi et al., 2022a).

The CHAOS campaign represents a first attempt at using the new SOARS wind-wave channel to isolate individual factors impacting SSA and INP emissions from seawater. Additional experiments with co-varying wind speed and wave amplitude are ongoing, focusing initially on measuring SSA (and not INP) concentrations. This is intended to generate realistic whitecap fraction-wind speed pairings to increase comparability with ambient data. Both SSA and INP concentrations measured by the CFDC increased with wind speed during CHAOS, as expected. IS measurements of INP concentration demonstrated a less clear trend with wind speed, which may be due to the use of separate inlets with different particle losses. The very low sampling height during CHAOS (0.6 m) relative to ambient (several to 20+ m) may have led to decreased losses of large particles, and requires further study before the comparability of such interfacial measurements to ambient marine boundary layer observations can be assessed. A mechanism involving spume droplet production of aggregate particles was proposed to explain the unexpected results of peroxide digestions of IS filters collected at high wind speeds, which also requires further

https://doi.org/10.5194/egusphere-2024-2159
Preprint. Discussion started: 25 July 2024

observations to evaluate. Following additional characterization of particle losses in SOARS and aerosol sampling inlets, and utilizing measurements with paired wind speed and whitecap fraction, future studies in the SOARS facility will be well poised to answer remaining questions about SSA and INP emissions as a function of wind speed, wave state, and temperature.

Data availability. Data presented in this study is in the process of being archived in the Dryad repository (https://datadryad.org/stash) and will be available online soon.

Appendix A

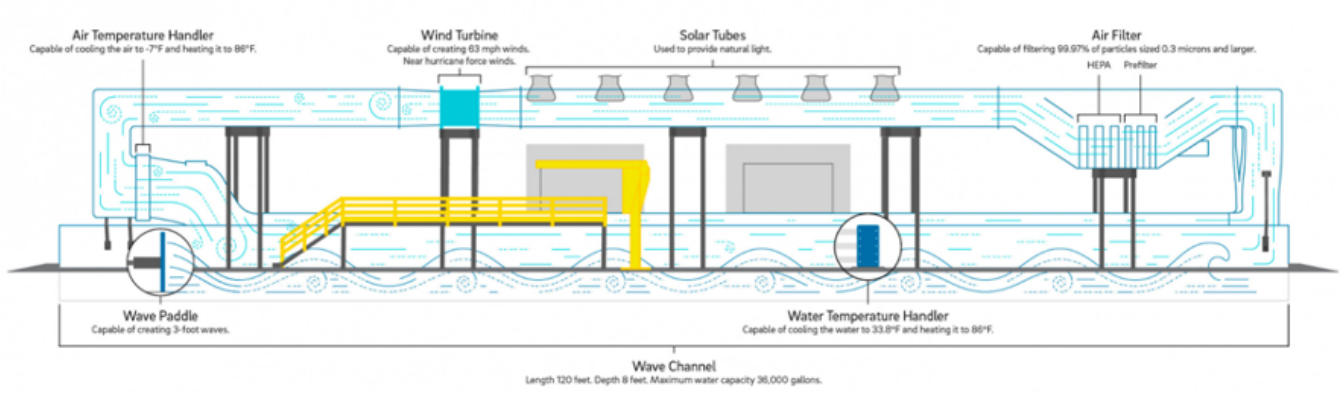

Figure A1. Schematic of the Scripps Ocean-Atmosphere Research Simulator (SOARS) wind-wave channel at the Scripps Institution of Oceanography showing key features relevant for SSA production and seawater biology.

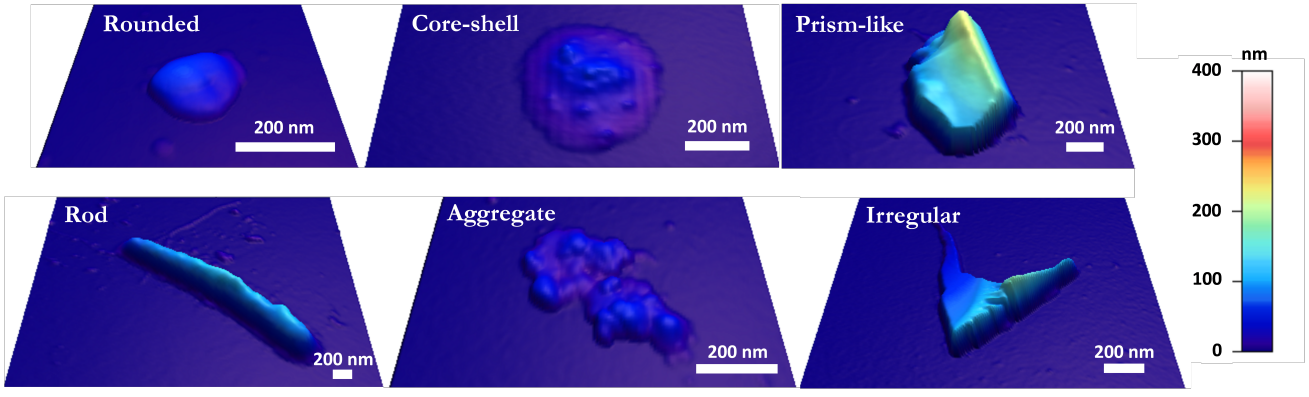

Figure A2. Selected illustrative AFM 3D-height images of six main particle morphological categories (rounded, core-shell, prism-like, rod, aggregate and irregular) identified at four wind speeds of 9.57, 16.28, 18.72, and 21.16 m s^{-1}. Images were all collected at 20 % RH.

https://doi.org/10.5194/egusphere-2024-2159
Preprint. Discussion started: 25 July 2024

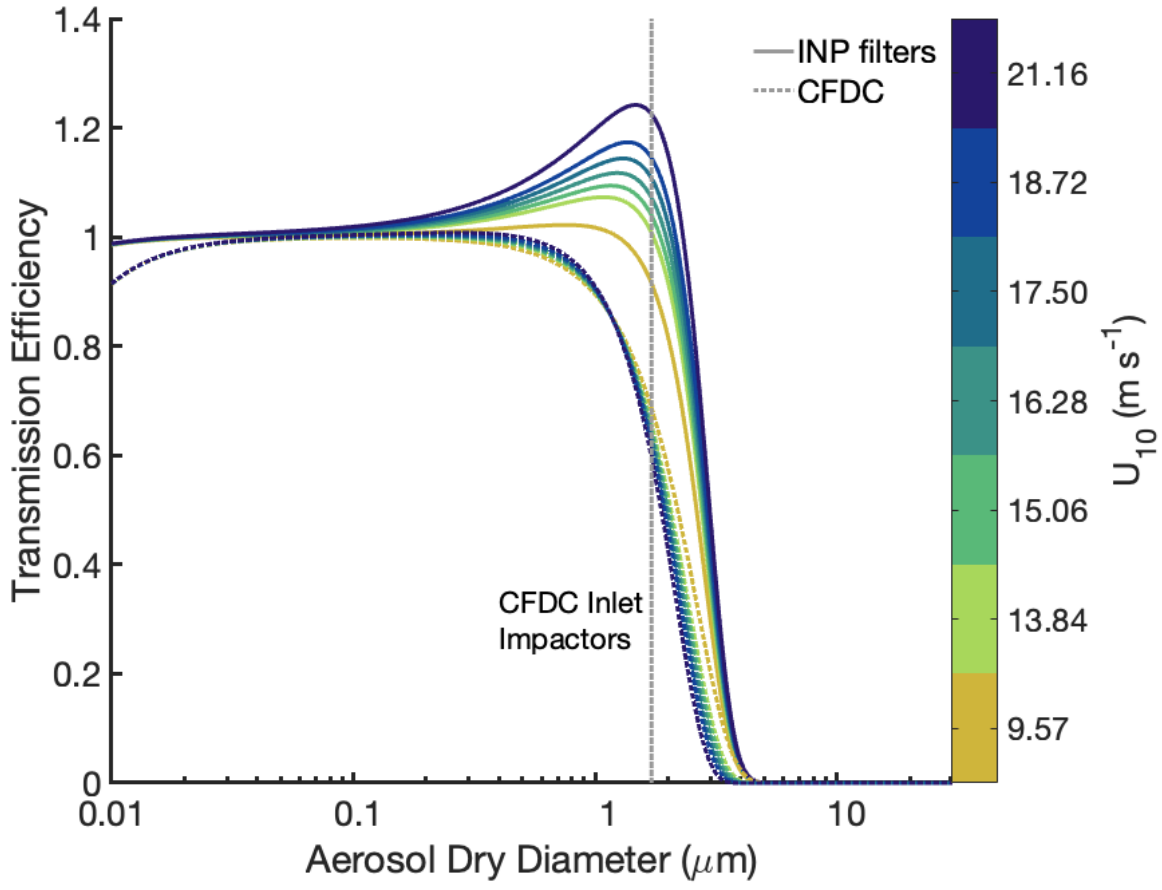

Figure A3. Estimated particle transmission efficiency during CHAOS for particles reaching either the CFDC (SEMS + APS) or INP filters (SMPS + APS), based on the different inlet geometries. These theoretical calculations used the von der Weiden et al. (2009) Particle Loss Calculator. Calculations were performed for the whole inlet in aerodynamic diameter, with a particle density ρ=1 and later corrected for expected particle density, water uptake, and shape factor (Sec. 2.3). Colors indicate the wind speed of the measurement, with INP filter curves in solid lines and CFDC curves in dashed lines.

https://doi.org/10.5194/egusphere-2024-2159
Preprint. Discussion started: 25 July 2024

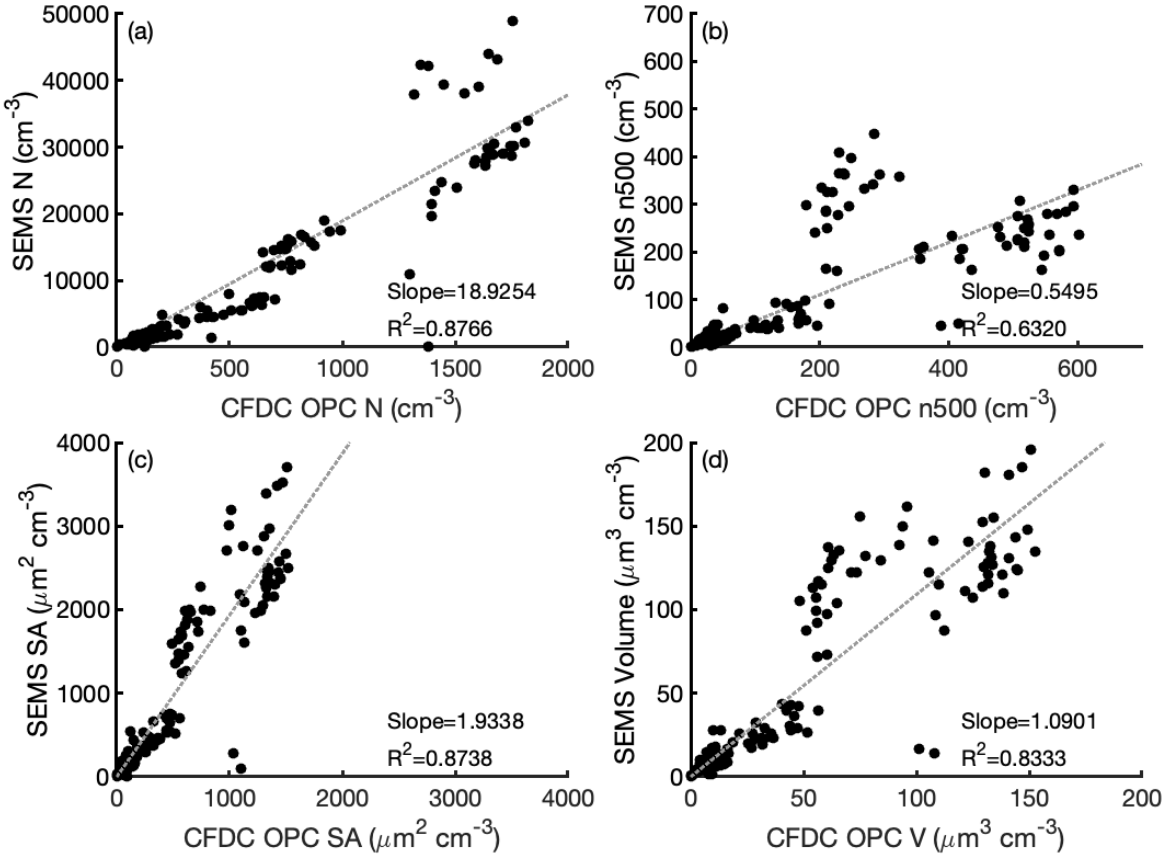

Figure A4. Correction factors derived for the CFDC OPC based on SEMS + APS aerosol measurements, for total particle number (a), n500 (b), particle surface area (c) and particle volume (d) concentrations.

https://doi.org/10.5194/egusphere-2024-2159
Preprint. Discussion started: 25 July 2024

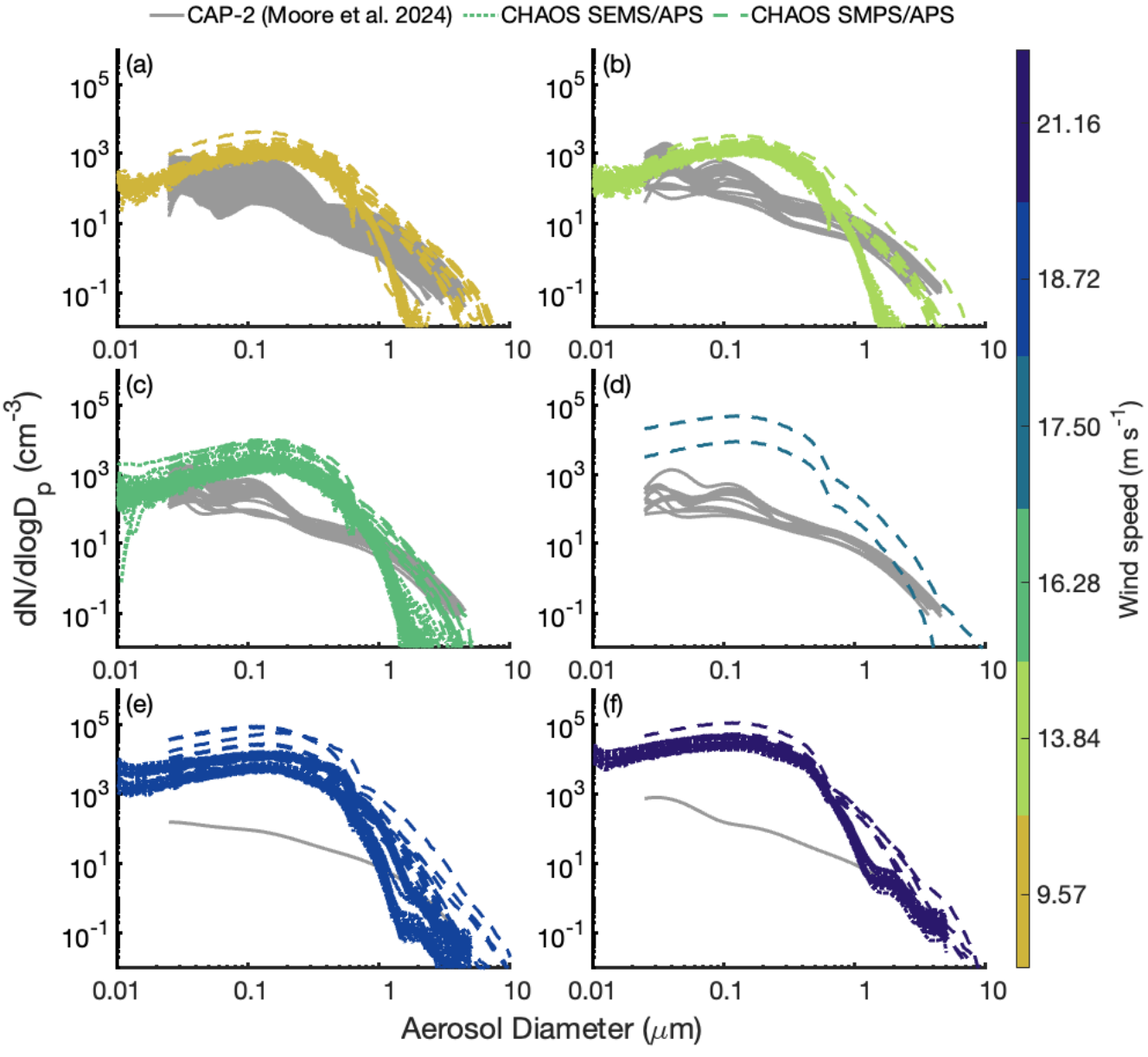

Figure A5. CHAOS aerosol size distributions at (a) 9.57 m s^{-1} (yellow), (b) 13.84 m s^{-1} (light green), (c) 16.28 m s^{-1} (green), (d) 17.50 m s^{-1} (light blue), (e) 18.72 m s^{-1} (dark blue), and (f) 21.16 m s^{-1} (dark purple). Measurements from the SEMS + APS are shown in the colored dotted lines, SMPS + APS observations in the colored dashed lines, and observations from CAP-2 (Moore et al., 2024), in the solid gray lines, if available. Measurements from CAP-2 are shown if they are within ±0.5 m s^{-1} of the SOARS U_{10} values.

https://doi.org/10.5194/egusphere-2024-2159
Preprint. Discussion started: 25 July 2024

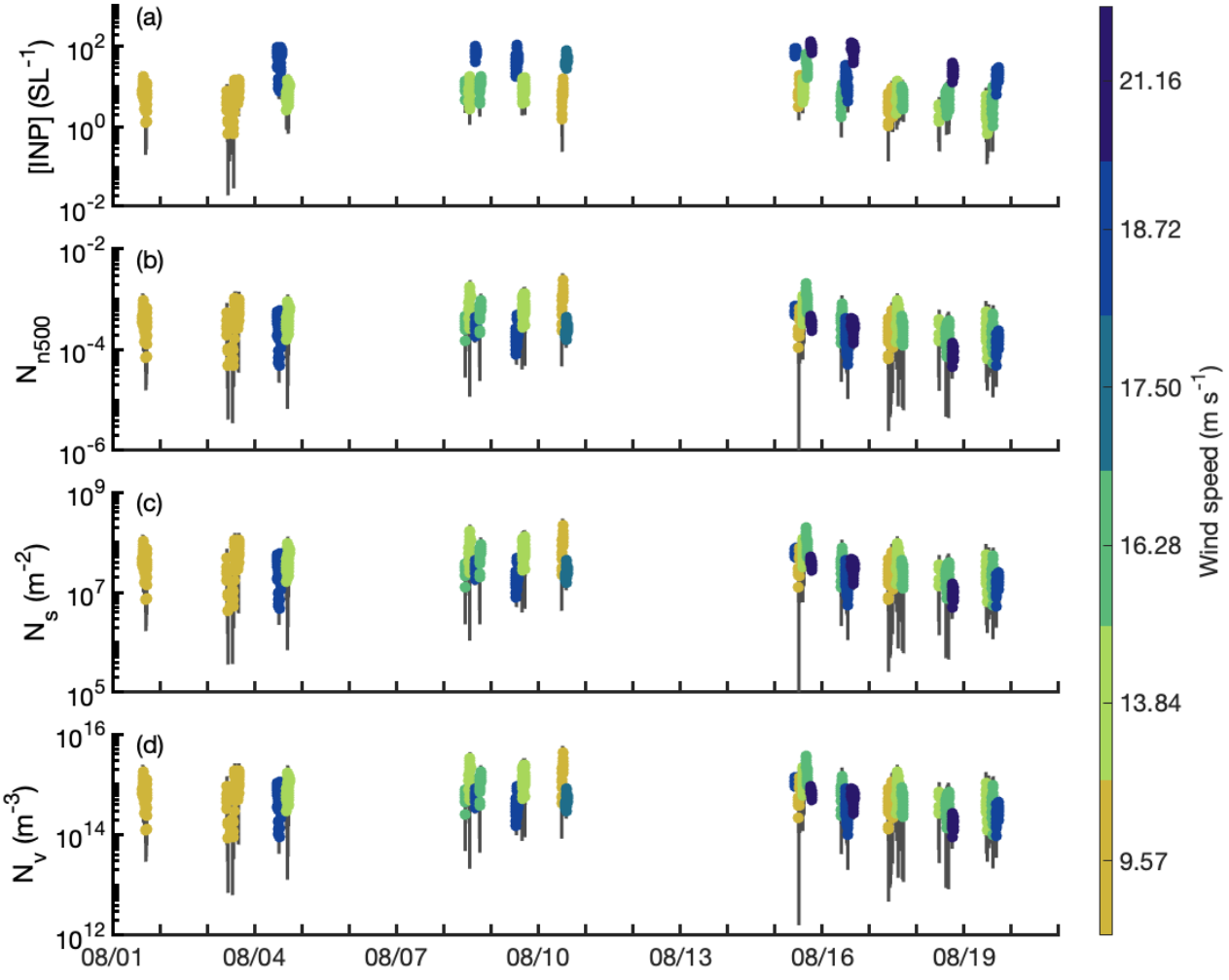

Figure A6. Time series of CFDC INP (a) number concentration, (b) normalized by n500 (N_{n500}), (c) normalized by aerosol surface area (N_s) and (d) normalized by aerosol volume (N_v) during CHAOS. Observations are colored by the wind speed during each measurement period.

https://doi.org/10.5194/egusphere-2024-2159
Preprint. Discussion started: 25 July 2024

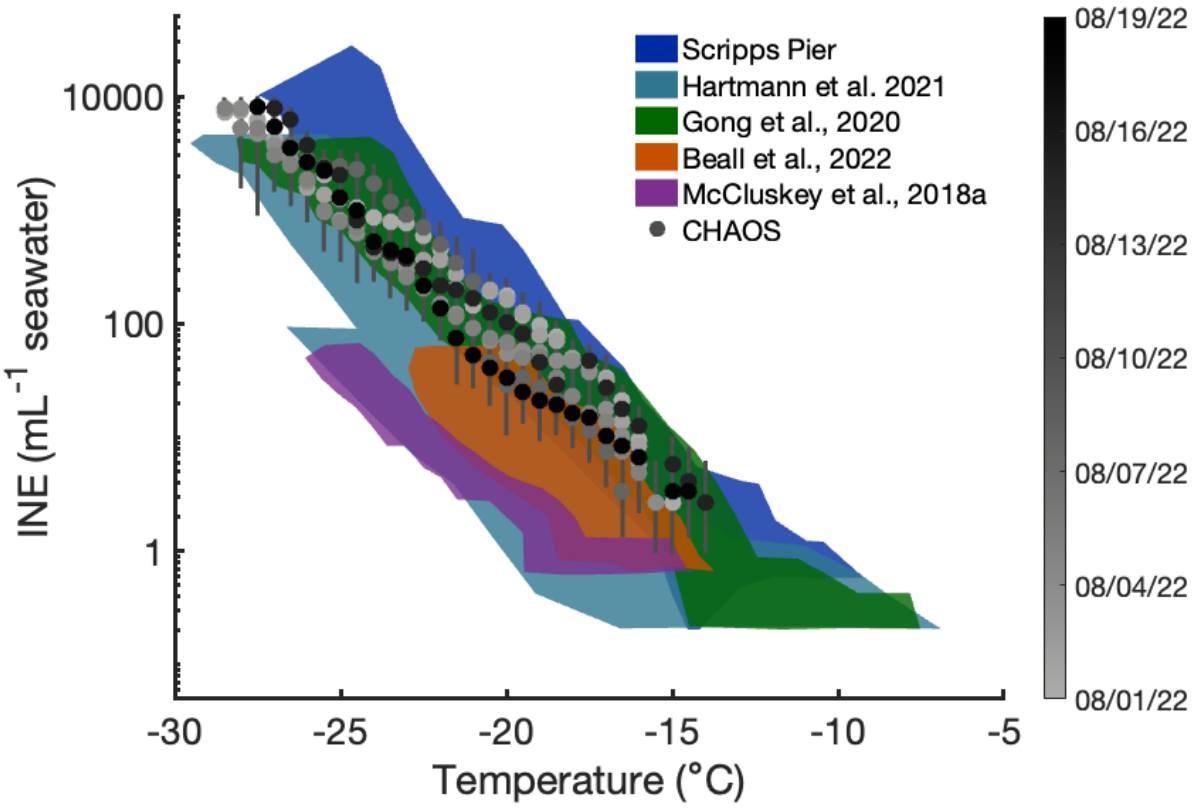

Figure A7. Seawater INE temperature spectra during CHAOS (grey circles), colored by collection date. Colored patches indicate comparisons with measurements from the Scripps Pier (dark blue), Barents Sea (Hartmann et al., 2021, light blue), mid-Atlantic (Gong et al., 2020, green), North Indian Ocean (Beall et al., 2022, orange), and Southern Ocean (McCluskey et al., 2018a, purple).

https://doi.org/10.5194/egusphere-2024-2159
Preprint. Discussion started: 25 July 2024

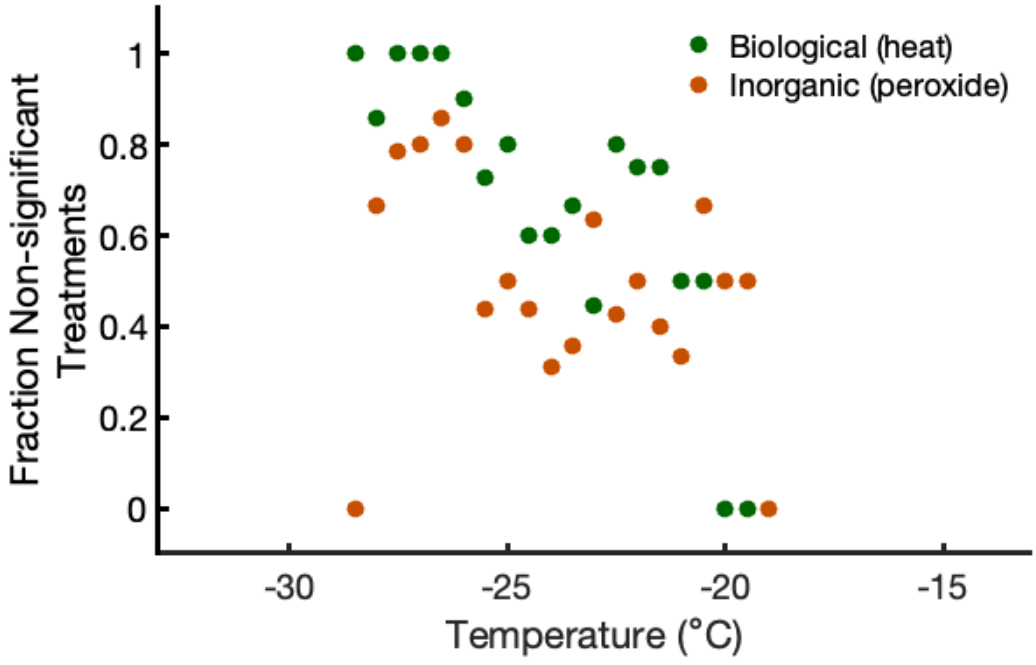

Figure A8. Fraction of INP filter treatment results that are not statistically different from the base spectra at the 95% confidence level. Results are shown as a function of temperature, with results for biological INPs (heat treatment) in green, and inorganic INPs (peroxide treatment) in orange.

https://doi.org/10.5194/egusphere-2024-2159
Preprint. Discussion started: 25 July 2024

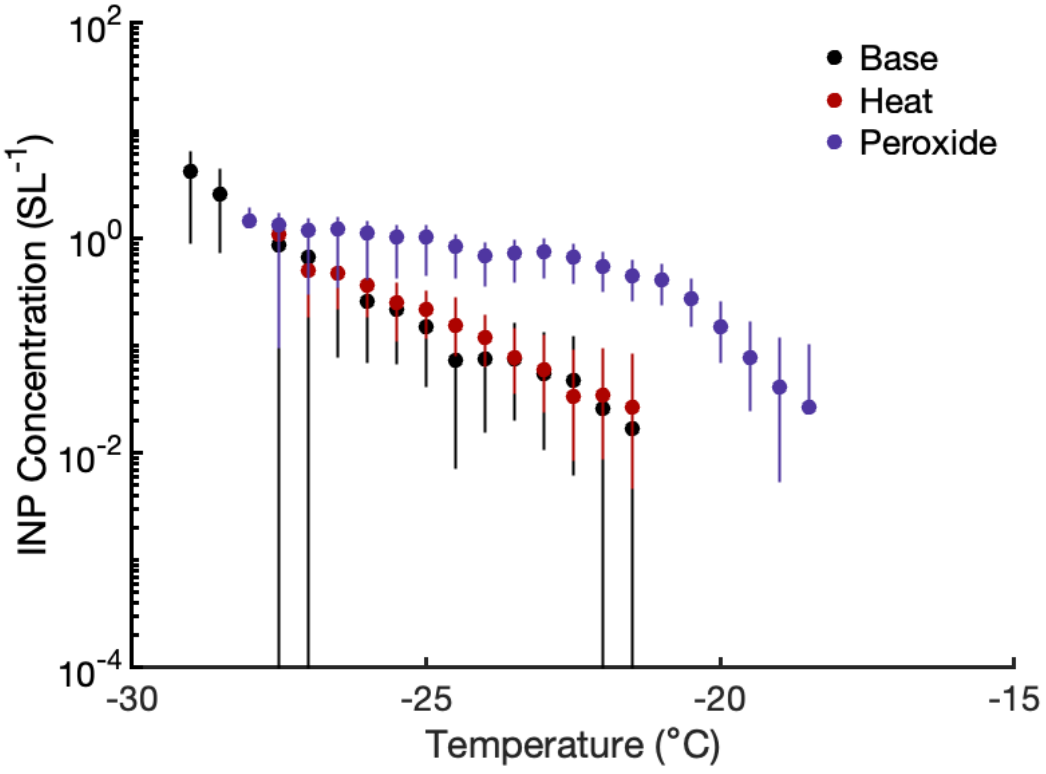

Figure A9. An example IS filter temperature spectra from 8/5/22 (18.72 m s^{-1}), with base measurements in black, heat-treated in red, and peroxide-treated in purple.

https://doi.org/10.5194/egusphere-2024-2159
Preprint. Discussion started: 25 July 2024

Table A1. Summary of the average (± one standard deviation) percentage of core-shell INPs with solid, semisolid, and liquid shells emitted at different wind speeds (9.57, 16.28, 18.72, and 21.16 m s^{-1}), as well as the average and range of viscoelastic response distances (VRD) measured for particles with semisolid shells. Measurements were made at 20 % and 60 % RH.

Wind speed (m s^{-1})	RH (%)	Solid (%)	Semisolid (%)	Liquid (%)	VRD* (nm)	VRD range* (nm)
9.57	20	60 ± 24	0	40 ± 26	N/A	N/A
	60	0	60 ± 26	40 ± 27	0.6 ± 0.1	0.5 – 0.7
16.28	20	95 ± 1	5 ± 1	0	0.6 ± 0.0	0.6
	60	47 ± 16	53 ± 16	0	0.8 ± 0.4	0.5 – 1.5
18.72	20	50 ± 24	42 ± 23	8 ± 1	2.7 ± 1.9	0.7 – 4.4
	60	14 ± 1	71 ± 22	14 ± 1	2.8 ± 2.3	0.8 – 5.4
21.16	20	46 ± 18	46 ± 18	8 ± 1	1.5 ± 1.2	0.5 – 3.6
	60	0	71 ± 21	29 ± 10	1.8 ± 1.6	0.5 – 3.8

*Data reported only for core-shell particles with organic coatings classified as semisolid

Author contributions. MDS, GBD, CL, and KAP designed the overall CHAOS campaign. KAM and PJD led the collection and processing of online INP measurements; KAM and TCJH led the collection and analysis of offline INP measurements, with assistance from SG. CKM and AVT led analyses and interpretation of AFM measurements of collected INPs. RJLIII and CDC led the collection and analysis of supplementary aerosol measurements. KAM and CKM created figures. KAM led the writing and editing of this article, with contributions from all the other authors.

Competing interests. There are no competing interests to declare.

Acknowledgements. This work was funded by the National Science Foundation (NSF) through the NSF Center for Aerosol Impacts on Chemistry of the Environment (CAICE) under award CHE-1801971. The authors thank the entire CHAOS team for their hard work throughout the campaign. Particular thanks are due to Joseph Mayer, Robert Klidy, and the team at the Scripps Institution of Oceanography Marine Science Development Center for their engineering support. KAM acknowledges support by an NSF Graduate Research Fellowship under Grant 006784. Any opinions, findings and conclusions or recommendations expressed in this material are those of the authors and do not necessarily reflect the views of the National Science Foundation.

https://doi.org/10.5194/egusphere-2024-2159
Preprint. Discussion started: 25 July 2024

References

Agresti, A. and Coull, B. A.: Approximate Is Better than "Exact" for Interval Estimation of Binomial Proportions, The American Statistician, 52, 119, https://doi.org/10.2307/2685469, 1998.

Alpert, P. A., Kilthau, W. P., O'Brien, R. E., Moffet, R. C., Gilles, M. K., Wang, B., Laskin, A., Aller, J. Y., and Knopf, D. A.: Ice-Nucleating Agents in Sea Spray Aerosol Identified and Quantified with a Holistic Multimodal Freezing Model, Science Advances, 8, eabq6842, https://doi.org/10.1126/sciadv.abq6842, 2022.

Andreae, M. O.: Aerosols Before Pollution, Science, 315, 50–51, https://doi.org/10.1126/science.1136529, 2007.

Ault, A. P., Moffet, R. C., Baltrusaitis, J., Collins, D. B., Ruppel, M. J., Cuadra-Rodriguez, L. A., Zhao, D., Guasco, T. L., Ebben, C. J., Geiger, F. M., Bertram, T. H., Prather, K. A., and Grassian, V. H.: Size-Dependent Changes in Sea Spray Aerosol Composition and Properties with Different Seawater Conditions, Environmental Science & Technology, 47, 5603–5612, https://doi.org/10.1021/es400416g, 2013.

Barry, K. R., Hill, T. C. J., Jentzsch, C., Moffett, B. F., Stratmann, F., and DeMott, P. J.: Pragmatic Protocols for Working Cleanly When Measuring Ice Nucleating Particles, Atmospheric Research, 250, 105 419, https://doi.org/10.1016/j.atmosres.2020.105419, 2021a.

Barry, K. R., Hill, T. C. J., Levin, E. J. T., Twohy, C. H., Moore, K. A., Weller, Z. D., Toohey, D. W., Reeves, M., Campos, T., Geiss, R., Schill, G. P., Fischer, E. V., Kreidenweis, S. M., and DeMott, P. J.: Observations of Ice Nucleating Particles in the Free Troposphere From Western US Wildfires, Journal of Geophysical Research: Atmospheres, 126, e2020JD033 752, https://doi.org/10.1029/2020JD033752, 2021b.

Barry, K. R., Hill, T. C. J., Nieto-Caballero, M., Douglas, T. A., Kreidenweis, S. M., DeMott, P. J., and Creamean, J. M.: Active Thermokarst Regions Contain Rich Sources of Ice Nucleating Particles, EGUsphere, pp. 1–19, https://doi.org/10.5194/egusphere-2023-1208, 2023.

Barthel, S., Tegen, I., and Wolke, R.: Do New Sea Spray Aerosol Source Functions Improve the Results of a Regional Aerosol Model?, Atmospheric Environment, 198, 265–278, https://doi.org/10.1016/j.atmosenv.2018.10.016, 2019.

Beall, C. M., Michaud, J. M., Fish, M. A., Dinasquet, J., Cornwell, G. C., Stokes, M. D., Burkart, M. D., Hill, T. C., DeMott, P. J., and Prather, K. A.: Cultivable Halotolerant Ice-Nucleating Bacteria and Fungi in Coastal Precipitation, Atmospheric Chemistry and Physics, 21, 9031–9045, https://doi.org/10.5194/acp-21-9031-2021, 2021.

Beall, C. M., Hill, T. C. J., DeMott, P. J., Köneman, T., Pikridas, M., Drewnick, F., Harder, H., Pöhlker, C., Lelieveld, J., Weber, B., Iakovides, M., Prokeš, R., Sciare, J., Andreae, M. O., Stokes, M. D., and Prather, K. A.: Ice-Nucleating Particles near Two Major Dust Source Regions, Atmospheric Chemistry and Physics, 22, 12 607–12 627, https://doi.org/10.5194/acp-22-12607-2022, 2022.

Bellouin, N., Quaas, J., Morcrette, J.-J., and Boucher, O.: Estimates of Aerosol Radiative Forcing from the MACC Re-Analysis, Atmospheric Chemistry and Physics, 13, 2045–2062, https://doi.org/10.5194/acp-13-2045-2013, 2013.

Bigg, E.: Long-Term Trends in Ice Nucleus Concentrations, Atmospheric Research, 25, 409–415, https://doi.org/10.1016/0169-8095(90)90025-8, 1990.

Bigg, E. K.: Ice Nucleus Concentrations in Remote Areas, Journal of the Atmospheric Sciences, 30, 1153–1157, https://doi.org/10.1175/1520-0469(1973)030<1153:INCIRA>2.0.CO;2, 1973.

Bjordal, J., Storelvmo, T., Alterskjær, K., and Carlsen, T.: Equilibrium Climate Sensitivity above 5 °C Plausible Due to State-Dependent Cloud Feedback, Nature Geoscience, 13, 718–721, https://doi.org/10.1038/s41561-020-00649-1, 2020.

Burrows, S. M., Hoose, C., Pöschl, U., and Lawrence, M. G.: Ice Nuclei in Marine Air: Biogenic Particles or Dust?, Atmospheric Chemistry and Physics, 13, 245–267, https://doi.org/10.5194/acp-13-245-2013, 2013.

https://doi.org/10.5194/egusphere-2024-2159
Preprint. Discussion started: 25 July 2024

Burrows, S. M., Easter, R., Liu, X., Ma, P.-L., Wang, H., Elliott, S. M., Singh, B., Zhang, K., and Rasch, P. J.: OCEANFILMS Sea-Spray Organic Aerosol Emissions – Part 1: Implementation and Impacts on Clouds, Atmospheric Chemistry and Physics Discussions, pp. 1–27, https://doi.org/10.5194/acp-2018-70, 2018.

Cappa, C. D., Asadi, S., Barreda, S., Wexler, A. S., Bouvier, N. M., and Ristenpart, W. D.: Expiratory Aerosol Particle Escape from Surgical Masks Due to Imperfect Sealing, Scientific Reports, 11, 12 110, https://doi.org/10.1038/s41598-021-91487-7, 2021.

Cappa, C. D., Ristenpart, W. D., Barreda, S., Bouvier, N. M., Levintal, E., Wexler, A. S., and Roman, S. A.: A Highly Efficient Cloth Facemask Design, Aerosol Science and Technology, 56, 12–28, https://doi.org/10.1080/02786826.2021.1962795, 2022.

Carslaw, K. S., Lee, L. A., Reddington, C. L., Pringle, K. J., Rap, A., Forster, P. M., Mann, G. W., Spracklen, D. V., Woodhouse, M. T., Regayre, L. A., and Pierce, J. R.: Large Contribution of Natural Aerosols to Uncertainty in Indirect Forcing, Nature, 503, 67–71, https://doi.org/10.1038/nature12674, 2013.

Carslaw, K. S., Gordon, H., Hamilton, D. S., Johnson, J. S., Regayre, L. A., Yoshioka, M., and Pringle, K. J.: Aerosols in the Pre-industrial Atmosphere, Current Climate Change Reports, 3, 1–15, https://doi.org/10.1007/s40641-017-0061-2, 2017.

Cesana, G. and Storelvmo, T.: Improving Climate Projections by Understanding How Cloud Phase Affects Radiation, Journal of Geophysical Research: Atmospheres, 122, 4594–4599, https://doi.org/10.1002/2017JD026927, 2017.

Chen, S., Qiao, F., Jiang, W., Guo, J., and Dai, D.: Impact of Surface Waves on Wind Stress under Low to Moderate Wind Conditions, Journal of Physical Oceanography, 49, 2017–2028, https://doi.org/10.1175/JPO-D-18-0266.1, 2019.

Chin, W.-C., Orellana, M. V., and Verdugo, P.: Spontaneous Assembly of Marine Dissolved Organic Matter into Polymer Gels, Nature, 391, 568–572, https://doi.org/10.1038/35345, 1998.

Christiansen, S., Salter, M. E., Gorokhova, E., Nguyen, Q. T., and Bilde, M.: Sea Spray Aerosol Formation: Laboratory Results on the Role of Air Entrainment, Water Temperature, and Phytoplankton Biomass, Environmental Science & Technology, 53, 13 107–13 116, https://doi.org/10.1021/acs.est.9b04078, 2019.

Cochran, R. E., Ryder, O. S., Grassian, V. H., and Prather, K. A.: Sea Spray Aerosol: The Chemical Link between the Oceans, Atmosphere, and Climate, Accounts of Chemical Research, 50, 599–604, https://doi.org/10.1021/acs.accounts.6b00603, 2017.

Creamean, J. M., Cross, J. N., Pickart, R., McRaven, L., Lin, P., Pacini, A., Hanlon, R., Schmale, D. G., Ceniceros, J., Aydell, T., Colombi, N., Bolger, E., and DeMott, P. J.: Ice Nucleating Particles Carried From Below a Phytoplankton Bloom to the Arctic Atmosphere, Geophysical Research Letters, 46, 8572–8581, https://doi.org/10.1029/2019GL083039, 2019.

de Leeuw, G., Andreas, E. L., Anguelova, M. D., Fairall, C. W., Lewis, E. R., O'Dowd, C., Schulz, M., and Schwartz, S. E.: Production Flux of Sea Spray Aerosol, Reviews of Geophysics, 49, https://doi.org/10.1029/2010RG000349, 2011.

Deike, L., Reichl, B. G., and Paulot, F.: A Mechanistic Sea Spray Generation Function Based on the Sea State and the Physics of Bubble Bursting, AGU Advances, 3, e2022AV000 750, https://doi.org/10.1029/2022AV000750, 2022.

DeMott, P. J., Prenni, A. J., McMeeking, G. R., Sullivan, R. C., Petters, M. D., Tobo, Y., Niemand, M., Möhler, O., Snider, J. R., Wang, Z., and Kreidenweis, S. M.: Integrating Laboratory and Field Data to Quantify the Immersion Freezing Ice Nucleation Activity of Mineral Dust Particles, Atmospheric Chemistry and Physics, 15, 393–409, https://doi.org/10.5194/acp-15-393-2015, 2015.

DeMott, P. J., Hill, T. C. J., McCluskey, C. S., Prather, K. A., Collins, D. B., Sullivan, R. C., Ruppel, M. J., Mason, R. H., Irish, V. E., Lee, T., Hwang, C. Y., Rhee, T. S., Snider, J. R., McMeeking, G. R., Dhaniyala, S., Lewis, E. R., Wentzell, J. J. B., Abbatt, J. P. D., Lee, C., Sultana, C. M., Ault, A. P., Axson, J. L., Diaz Martinez, M., Venero, I., Santos-Figueroa, G., Stokes, M. D., Deane, G. B., Mayol-Bracero, O. L., Grassian, V. H., Bertram, T. H., Bertram, A. K., Moffett, B. F., and Franc, G. D.: Sea Spray Aerosol as a Unique Source of Ice Nucleating Particles, Proceedings of the National Academy of Sciences, 113, 5797–5803, https://doi.org/10.1073/pnas.1514034112, 2016.

https://doi.org/10.5194/egusphere-2024-2159
Preprint. Discussion started: 25 July 2024

DeMott, P. J., Hill, T. C. J., Petters, M. D., Bertram, A. K., Tobo, Y., Mason, R. H., Suski, K. J., McCluskey, C. S., Levin, E. J. T., Schill, G. P., Boose, Y., Rauker, A. M., Miller, A. J., Zaragoza, J., Rocci, K., Rothfuss, N. E., Taylor, H. P., Hader, J. D., Chou, C., Huffman, J. A., Pöschl, U., Prenni, A. J., and Kreidenweis, S. M.: Comparative Measurements of Ambient Atmospheric Concentrations of Ice Nucleating Particles Using Multiple Immersion Freezing Methods and a Continuous Flow Diffusion Chamber, Atmospheric Chemistry and Physics, 17, 11 227–11 245, https://doi.org/10.5194/acp-17-11227-2017, 2017.

DeMott, P. J., Möhler, O., Cziczo, D. J., Hiranuma, N., Petters, M. D., Petters, S. S., Belosi, F., Bingemer, H. G., Brooks, S. D., Budke, C., Burkert-Kohn, M., Collier, K. N., Danielczok, A., Eppers, O., Felgitsch, L., Garimella, S., Grothe, H., Herenz, P., Hill, T. C. J., Höhler, K., Kanji, Z. A., Kiselev, A., Koop, T., Kristensen, T. B., Krüger, K., Kulkarni, G., Levin, E. J. T., Murray, B. J., Nicosia, A., O'Sullivan, D., Peckhaus, A., Polen, M. J., Price, H. C., Reicher, N., Rothenberg, D. A., Rudich, Y., Santachiara, G., Schiebel, T., Schrod, J., Seifried, T. M., Stratmann, F., Sullivan, R. C., Suski, K. J., Szakáll, M., Taylor, H. P., Ullrich, R., Vergara-Temprado, J., Wagner, R., Whale, T. F., Weber, D., Welti, A., Wilson, T. W., Wolf, M. J., and Zenker, J.: The Fifth International Workshop on Ice Nucleation Phase 2 (FIN-02): Laboratory Intercomparison of Ice Nucleation Measurements, Atmospheric Measurement Techniques, 11, 6231–6257, https://doi.org/10.5194/amt-11-6231-2018, 2018.

DeMott, P. J., Hill, T. C. J., Moore, K. A., Perkins, R. J., Mael, L. E., Busse, H. L., Lee, H., Kaluarachchi, C. P., Mayer, K. J., Sauer, J. S., Mitts, B. A., Tivanski, A. V., Grassian, V. H., Cappa, C. D., Bertram, T. H., and Prather, K. A.: Atmospheric Oxidation Impact on Sea Spray Produced Ice Nucleating Particles, Environmental Science: Atmospheres, 3, 1513–1532, https://doi.org/10.1039/D3EA00060E, 2023.

Engel, A., Bange, H. W., Cunliffe, M., Burrows, S. M., Friedrichs, G., Galgani, L., Herrmann, H., Hertkorn, N., Johnson, M., Liss, P. S., Quinn, P. K., Schartau, M., Soloviev, A., Stolle, C., Upstill-Goddard, R. C., van Pinxteren, M., and Zäncker, B.: The Ocean's Vital Skin: Toward an Integrated Understanding of the Sea Surface Microlayer, Frontiers in Marine Science, 4, 165, https://doi.org/10.3389/fmars.2017.00165, 2017.

Fall, R. and Schnell, R.: Association of an Ice-Nucleating Pseudomonad with Cultures of the Marine Dinoflagellate, Heterocapsa Niei, Journal of Marine Research, 43, 1985.

Forestieri, S. D., Moore, K. A., Borrero, R. M., Wang, A., Stokes, M. D., and Cappa, C. D.: Temperature and Composition Dependence of Sea Spray Aerosol Production, Geophysical Research Letters, 45, 7218–7225, https://doi.org/10.1029/2018GL078193, 2018.

Forster, P., Storelvmo, T., Armour, K., Collins, W., Dufresne, J.-L., Frame, D., Lunt, D. J., Mauritsen, T., Palmer, M. D., Watanabe, M., Wild, M., and Zhang, X.: The Earth's Energy Budget, Climate Feedbacks, and Climate Sensitivity, in: Climate Change 2021: The Physical Science Basis. Contribution of Working Group I to the Sixth Assessment Report of the Intergovernmental Panel on Climate Change, edited by Masson-Delmotte, V., Zhai, P., Pirani, A., Connors, S. L., Péan, C., Berger, S., Caud, N., Chen, Y., Goldfarb, L., Gomis, M. I., Huang, M., Leitzell, K., Lonnoy, E., Matthews, J. B. R., Maycock, T. K., Waterfield, T., Yelekçi, Ö., Yu, R., and Zhou, B., pp. 923–1054, Cambridge University Press, Cambridge, United Kingdom and New York, NY, USA, https://doi.org/10.1017/9781009157896.001, 2021.

Fröhlich-Nowoisky, J., Hill, T. C. J., Pummer, B. G., Yordanova, P., Franc, G. D., and Pöschl, U.: Ice Nucleation Activity in the Widespread Soil Fungus *Mortierella Alpina*, Biogeosciences, 12, 1057–1071, https://doi.org/10.5194/bg-12-1057-2015, 2015.

Fuentes, E., Coe, H., Green, D., de Leeuw, G., and McFiggans, G.: On the Impacts of Phytoplankton-Derived Organic Matter on the Properties of the Primary Marine Aerosol – Part 1: Source Fluxes, Atmospheric Chemistry and Physics, 10, 9295–9317, https://doi.org/10.5194/acp-10-9295-2010, 2010.

Gong, S. L.: A Parameterization of Sea-Salt Aerosol Source Function for Sub- and Super-Micron Particles, Global Biogeochemical Cycles, 17, https://doi.org/10.1029/2003GB002079, 2003.

https://doi.org/10.5194/egusphere-2024-2159
Preprint. Discussion started: 25 July 2024

Gong, X., Wex, H., van Pinxteren, M., Triesch, N., Fomba, K. W., Lubitz, J., Stolle, C., Robinson, T.-B., Müller, T., Herrmann, H., and Stratmann, F.: Characterization of Aerosol Particles at Cabo Verde Close to Sea Level and at the Cloud Level – Part 2: Ice-nucleating Particles in Air, Cloud and Seawater, Atmospheric Chemistry and Physics, 20, 1451–1468, https://doi.org/10.5194/acp-20-1451-2020, 2020.

Gryspeerdt, E., Povey, A. C., Grainger, R. G., Hasekamp, O., Hsu, N. C., Mulcahy, J. P., Sayer, A. M., and Sorooshian, A.: Uncertainty in Aerosol–Cloud Radiative Forcing Is Driven by Clean Conditions, Atmospheric Chemistry and Physics, 23, 4115–4122, https://doi.org/10.5194/acp-23-4115-2023, 2023.

Grythe, H., Ström, J., Krejci, R., Quinn, P., and Stohl, A.: A Review of Sea-Spray Aerosol Source Functions Using a Large Global Set of Sea Salt Aerosol Concentration Measurements, Atmospheric Chemistry and Physics, 14, 1277–1297, https://doi.org/10.5194/acp-14-1277-2014, 2014.

Hartery, S., Toohey, D., Revell, L., Sellegri, K., Kuma, P., Harvey, M., and McDonald, A. J.: Constraining the Surface Flux of Sea Spray Particles From the Southern Ocean, Journal of Geophysical Research: Atmospheres, 125, e2019JD032026, https://doi.org/10.1029/2019JD032026, 2020.

Hartmann, M., Adachi, K., Eppers, O., Haas, C., Herber, A., Holzinger, R., Hünerbein, A., Jäkel, E., Jentzsch, C., van Pinxteren, M., Wex, H., Willmes, S., and Stratmann, F.: Wintertime Airborne Measurements of Ice Nucleating Particles in the High Arctic: A Hint to a Marine, Biogenic Source for Ice Nucleating Particles, Geophysical Research Letters, 47, e2020GL087770, https://doi.org/10.1029/2020GL087770, 2020.

Hartmann, M., Gong, X., Kecorius, S., van Pinxteren, M., Vogl, T., Welti, A., Wex, H., Zeppenfeld, S., Herrmann, H., Wiedensohler, A., and Stratmann, F.: Terrestrial or Marine – Indications towards the Origin of Ice-Nucleating Particles during Melt Season in the European Arctic up to 83.7° N, Atmospheric Chemistry and Physics, 21, 11613–11636, https://doi.org/10.5194/acp-21-11613-2021, 2021.

Heinze, C., Eyring, V., Friedlingstein, P., Jones, C., Balkanski, Y., Collins, W., Fichefet, T., Gao, S., Hall, A., Ivanova, D., Knorr, W., Knutti, R., Löw, A., Ponater, M., Schultz, M. G., Schulz, M., Siebesma, P., Teixeira, J., Tselioudis, G., and Vancoppenolle, M.: ESD Reviews: Climate Feedbacks in the Earth System and Prospects for Their Evaluation, Earth System Dynamics, 10, 379–452, https://doi.org/10.5194/esd-10-379-2019, 2019.

Hill, T. C. J., DeMott, P. J., Tobo, Y., Fröhlich-Nowoisky, J., Moffett, B. F., Franc, G. D., and Kreidenweis, S. M.: Sources of Organic Ice Nucleating Particles in Soils, Atmospheric Chemistry and Physics, 16, 7195–7211, https://doi.org/10.5194/acp-16-7195-2016, 2016.

Hill, T. C. J., Malfatti, F., McCluskey, C. S., Schill, G. P., Santander, M. V., Moore, K. A., Rauker, A. M., Perkins, R. J., Celussi, M., Levin, E. J. T., Suski, K. J., Cornwell, G. C., Lee, C., Negro, P. D., Kreidenweis, S. M., Prather, K. A., and DeMott, P. J.: Resolving the Controls over the Production and Emission of Ice-Nucleating Particles in Sea Spray, Environmental Science: Atmospheres, 3, 970–990, https://doi.org/10.1039/D2EA00154C, 2023.

Hiranuma, N., Augustin-Bauditz, S., Bingemer, H., Budke, C., Curtius, J., Danielczok, A., Diehl, K., Dreischmeier, K., Ebert, M., Frank, F., Hoffmann, N., Kandler, K., Kiselev, A., Koop, T., Leisner, T., Möhler, O., Nillius, B., Peckhaus, A., Rose, D., Weinbruch, S., Wex, H., Boose, Y., DeMott, P. J., Hader, J. D., Hill, T. C. J., Kanji, Z. A., Kulkarni, G., Levin, E. J. T., McCluskey, C. S., Murakami, M., Murray, B. J., Niedermeier, D., Petters, M. D., O'Sullivan, D., Saito, A., Schill, G. P., Tajiri, T., Tolbert, M. A., Welti, A., Whale, T. F., Wright, T. P., and Yamashita, K.: A Comprehensive Laboratory Study on the Immersion Freezing Behavior of Illite NX Particles: A Comparison of 17 Ice Nucleation Measurement Techniques, Atmospheric Chemistry and Physics, 15, 2489–2518, https://doi.org/10.5194/acp-15-2489-2015, 2015.

https://doi.org/10.5194/egusphere-2024-2159
Preprint. Discussion started: 25 July 2024

Hsu, S. A., Meindl, E. A., and Gilhousen, D. B.: Determining the Power-Law Wind-Profile Exponent under Near-Neutral Stability Conditions at Sea, Journal of Applied Meteorology and Climatology, 33, 757–765, https://doi.org/10.1175/1520-0450(1994)033<0757:DTPLWP>2.0.CO;2, 1994.

Huang, W. T. K., Ickes, L., Tegen, I., Rinaldi, M., Ceburnis, D., and Lohmann, U.: Global Relevance of Marine Organic Aerosol as Ice Nucleating Particles, Atmospheric Chemistry and Physics, 18, 11 423–11 445, https://doi.org/10.5194/acp-18-11423-2018, 2018.

Ickes, L., Porter, G. C. E., Wagner, R., Adams, M. P., Bierbauer, S., Bertram, A. K., Bilde, M., Christiansen, S., Ekman, A. M. L., Gorokhova, E., Höhler, K., Kiselev, A. A., Leck, C., Möhler, O., Murray, B. J., Schiebel, T., Ullrich, R., and Salter, M. E.: The Ice-Nucleating Activity of Arctic Sea Surface Microlayer Samples and Marine Algal Cultures, Atmospheric Chemistry and Physics, 20, 11 089–11 117, https://doi.org/10.5194/acp-20-11089-2020, 2020.

Irish, V. E., Elizondo, P., Chen, J., Chou, C., Charette, J., Lizotte, M., Ladino, L. A., Wilson, T. W., Gosselin, M., Murray, B. J., Polishchuk, E., Abbatt, J. P. D., Miller, L. A., and Bertram, A. K.: Ice-Nucleating Particles in Canadian Arctic Sea-Surface Microlayer and Bulk Seawater, Atmospheric Chemistry and Physics, 17, 10 583–10 595, https://doi.org/10.5194/acp-17-10583-2017, 2017.

Irish, V. E., Hanna, S. J., Willis, M. D., China, S., Thomas, J. L., Wentzell, J. J. B., Cirisan, A., Si, M., Leaitch, W. R., Murphy, J. G., Abbatt, J. P. D., Laskin, A., Girard, E., and Bertram, A. K.: Ice Nucleating Particles in the Marine Boundary Layer in the Canadian Arctic during Summer 2014, Atmospheric Chemistry and Physics, 19, 1027–1039, https://doi.org/10.5194/acp-19-1027-2019, 2019.

Jaeglé, L., Quinn, P. K., Bates, T. S., Alexander, B., and Lin, J.-T.: Global Distribution of Sea Salt Aerosols: New Constraints from in Situ and Remote Sensing Observations, Atmospheric Chemistry and Physics, 11, 3137–3157, https://doi.org/10.5194/acp-11-3137-2011, 2011.

Jio, D. A.: An Examination of the Seawater Aquarium System at Scripps Institution of Oceanography, Ph.D. thesis, UC San Diego, 2022.

Johnson, J. S., Regayre, L. A., Yoshioka, M., Pringle, K. J., Turnock, S. T., Browse, J., Sexton, D. M. H., Rostron, J. W., Schutgens, N. A. J., Partridge, D. G., Liu, D., Allan, J. D., Coe, H., Ding, A., Cohen, D. D., Atanacio, A., Vakkari, V., Asmi, E., and Carslaw, K. S.: Robust Observational Constraint of Uncertain Aerosol Processes and Emissions in a Climate Model and the Effect on Aerosol Radiative Forcing, Atmospheric Chemistry and Physics, 20, 9491–9524, https://doi.org/10.5194/acp-20-9491-2020, 2020.

Kaluarachchi, C. P., Or, V. W., Lan, Y., Hasenecz, E. S., Kim, D., Madawala, C. K., Dorcé, G. P., Mayer, K. J., Sauer, J. S., Lee, C., Cappa, C. D., Bertram, T. H., Stone, E. A., Prather, K. A., Grassian, V. H., and Tivanski, A. V.: Effects of Atmospheric Aging Processes on Nascent Sea Spray Aerosol Physicochemical Properties, ACS Earth and Space Chemistry, 6, 2732–2744, https://doi.org/10.1021/acsearthspacechem.2c00258, 2022a.

Kaluarachchi, C. P., Or, V. W., Lan, Y., Madawala, C. K., Hasenecz, E. S., Crocker, D. R., Morris, C. K., Lee, H. D., Mayer, K. J., Sauer, J. S., Lee, C., Dorce, G., Malfatti, F., Stone, E. A., Cappa, C. D., Grassian, V. H., Prather, K. A., and Tivanski, A. V.: Size-Dependent Morphology, Composition, Phase State, and Water Uptake of Nascent Submicrometer Sea Spray Aerosols during a Phytoplankton Bloom, ACS Earth and Space Chemistry, 6, 116–130, https://doi.org/10.1021/acsearthspacechem.1c00306, 2022b.

Kanji, Z. A., Ladino, L. A., Wex, H., Boose, Y., Burkert-Kohn, M., Cziczo, D. J., and Krämer, M.: Overview of Ice Nucleating Particles, Meteorological Monographs, 58, 1.1–1.33, https://doi.org/10.1175/AMSMONOGRAPHS-D-16-0006.1, 2017.

Kawana, K., Taketani, F., Matsumoto, K., Tobo, Y., Iwamoto, Y., Miyakawa, T., Ito, A., and Kanaya, Y.: Roles of Marine Biota in the Formation of Atmospheric Bioaerosols, Cloud Condensation Nuclei, and Ice-Nucleating Particles over the North Pacific Ocean, Bering Sea, and Arctic Ocean, Atmospheric Chemistry and Physics, 24, 1777–1799, https://doi.org/10.5194/acp-24-1777-2024, 2024.

Knopf, D. A., Alpert, P. A., Wang, B., and Aller, J. Y.: Stimulation of Ice Nucleation by Marine Diatoms, Nature Geoscience, 4, 88–90, https://doi.org/10.1038/ngeo1037, 2011.

https://doi.org/10.5194/egusphere-2024-2159
Preprint. Discussion started: 25 July 2024

Krishnamoorthy, K. and Lee, M.: New Approximate Confidence Intervals for the Difference between Two Poisson Means and Comparison, Journal of Statistical Computation and Simulation, 83, 2232–2243, https://doi.org/10.1080/00949655.2012.686616, 2012.

Ladino, L. A., Yakobi-Hancock, J. D., Kilthau, W. P., Mason, R. H., Si, M., Li, J., Miller, L. A., Schiller, C. L., Huffman, J. A., Aller, J. Y., Knopf, D. A., Bertram, A. K., and Abbatt, J. P. D.: Addressing the Ice Nucleating Abilities of Marine Aerosol: A Combination of Deposition Mode Laboratory and Field Measurements, Atmospheric Environment, 132, 1–10, https://doi.org/10.1016/j.atmosenv.2016.02.028, 2016.

Lamont-Smith, T. and Waseda, T.: Wind Wave Growth at Short Fetch, Journal of Physical Oceanography, 38, 1597–1606, https://doi.org/10.1175/2007JPO3712.1, 2008.

Lapere, R., Thomas, J. L., Marelle, L., Ekman, A. M. L., Frey, M. M., Lund, M. T., Makkonen, R., Ranjithkumar, A., Salter, M. E., Samset, B. H., Schulz, M., Sogacheva, L., Yang, X., and Zieger, P.: The Representation of Sea Salt Aerosols and Their Role in Polar Climate Within CMIP6, Journal of Geophysical Research: Atmospheres, 128, e2022JD038 235, https://doi.org/10.1029/2022JD038235, 2023.

Lee, H. D., Ray, K. K., and Tivanski, A. V.: Solid, Semisolid, and Liquid Phase States of Individual Submicrometer Particles Directly Probed Using Atomic Force Microscopy, Analytical Chemistry, 89, 12 720–12 726, https://doi.org/10.1021/acs.analchem.7b02755, 2017.

Lee, H. D., Morris, H. S., Laskina, O., Sultana, C. M., Lee, C., Jayarathne, T., Cox, J. L., Wang, X., Hasenecz, E. S., DeMott, P. J., Bertram, T. H., Cappa, C. D., Stone, E. A., Prather, K. A., Grassian, V. H., and Tivanski, A. V.: Organic Enrichment, Physical Phase State, and Surface Tension Depression of Nascent Core–Shell Sea Spray Aerosols during Two Phytoplankton Blooms, ACS Earth and Space Chemistry, 4, 650–660, https://doi.org/10.1021/acsearthspacechem.0c00032, 2020.

Lewis, E. R. and Schwartz, S. E.: Sea Salt Aerosol Production: Mechanisms, Methods, Measurements and Models—A Critical Review, vol. 152 of *Geophysical Monograph*, American Geophysical Union, Washington, DC, ISBN 978-0-87590-417-7, 2004.

Lin, Y., Fan, J., Li, P., Leung, L.-y. R., DeMott, P. J., Goldberger, L., Comstock, J., Liu, Y., Jeong, J.-H., and Tomlinson, J.: Modeling Impacts of Ice-Nucleating Particles from Marine Aerosols on Mixed-Phase Orographic Clouds during 2015 ACAPEX Field Campaign, Atmospheric Chemistry and Physics, 22, 6749–6771, https://doi.org/10.5194/acp-22-6749-2022, 2022.

Liu, S., Liu, C.-C., Froyd, K. D., Schill, G. P., Murphy, D. M., Bui, T. P., Dean-Day, J. M., Weinzierl, B., Dollner, M., Diskin, G. S., Chen, G., and Gao, R.-S.: Sea Spray Aerosol Concentration Modulated by Sea Surface Temperature, Proceedings of the National Academy of Sciences, 118, https://doi.org/10.1073/pnas.2020583118, 2021.

Madawala, C. K., Lee, H. D., Kaluarachchi, C. P., and Tivanski, A. V.: Probing the Water Uptake and Phase State of Individual Sucrose Nanoparticles Using Atomic Force Microscopy, ACS Earth and Space Chemistry, 5, 2612–2620, https://doi.org/10.1021/acsearthspacechem.1c00101, 2021.

Madawala, C. K., Molina, C., Kim, D., Kirindigoda Gamage, D., Sun, M., Leibensperger III, R. J., Mehndiratta, L., Lee, J., Kaluarachchi, C. P., Kimble, K. A., Sandstrom, G., Harb, C., Dinasquet, J., Malfatti, F., Prather, K. A., Deane, G. B., Stokes, M. D., Lee, C., Slade, J. H., Stone, E. A., Grassian, V. H., and Tivanski, A. V.: The Effects of Wind Speed on Size-Dependent Morphology and Composition of Sea Spray Aerosols., ACS Earth and Space Chemistry, 2024, in review.

Mårtensson, E. M., Nilsson, E. D., de Leeuw, G., Cohen, L. H., and Hansson, H.-C.: Laboratory Simulations and Parameterization of the Primary Marine Aerosol Production, Journal of Geophysical Research: Atmospheres, 108, https://doi.org/10.1029/2002JD002263, 2003.

May, N. W., Axson, J. L., Watson, A., Pratt, K. A., and Ault, A. P.: Lake Spray Aerosol Generation: A Method for Producing Representative Particles from Freshwater Wave Breaking, Atmospheric Measurement Techniques, 9, 4311–4325, https://doi.org/10.5194/amt-9-4311-2016, 2016.

https://doi.org/10.5194/egusphere-2024-2159
Preprint. Discussion started: 25 July 2024

Mayer, K. J., Wang, X., Santander, M. V., Mitts, B. A., Sauer, J. S., Sultana, C. M., Cappa, C. D., and Prather, K. A.: Secondary Marine Aerosol Plays a Dominant Role over Primary Sea Spray Aerosol in Cloud Formation, ACS Central Science, 6, 2259–2266, https://doi.org/10.1021/acscentsci.0c00793, 2020.

McCluskey, C. S., DeMott, P. J., Prenni, A. J., Levin, E. J. T., McMeeking, G. R., Sullivan, A. P., Hill, T. C. J., Nakao, S., Carrico, C. M., and Kreidenweis, S. M.: Characteristics of Atmospheric Ice Nucleating Particles Associated with Biomass Burning in the US: Prescribed Burns and Wildfires, Journal of Geophysical Research: Atmospheres, 119, 10 458–10 470, https://doi.org/10.1002/2014JD021980, 2014.

McCluskey, C. S., Hill, T. C. J., Humphries, R. S., Rauker, A. M., Moreau, S., Strutton, P. G., Chambers, S. D., Williams, A. G., McRobert, I., Ward, J., Keywood, M. D., Harnwell, J., Ponsonby, W., Loh, Z. M., Krummel, P. B., Protat, A., Kreidenweis, S. M., and DeMott, P. J.: Observations of Ice Nucleating Particles Over Southern Ocean Waters, Geophysical Research Letters, 45, 11,989–11,997, https://doi.org/10.1029/2018GL079981, 2018a.

McCluskey, C. S., Hill, T. C. J., Sultana, C. M., Laskina, O., Trueblood, J., Santander, M. V., Beall, C. M., Michaud, J. M., Kreidenweis, S. M., Prather, K. A., Grassian, V., and DeMott, P. J.: A Mesocosm Double Feature: Insights into the Chemical Makeup of Marine Ice Nucleating Particles, Journal of the Atmospheric Sciences, 75, 2405–2423, https://doi.org/10.1175/JAS-D-17-0155.1, 2018b.

McCluskey, C. S., Ovadnevaite, J., Rinaldi, M., Atkinson, J., Belosi, F., Ceburnis, D., Marullo, S., Hill, T. C. J., Lohmann, U., Kanji, Z. A., O'Dowd, C., Kreidenweis, S. M., and DeMott, P. J.: Marine and Terrestrial Organic Ice-Nucleating Particles in Pristine Marine to Continentally Influenced Northeast Atlantic Air Masses, Journal of Geophysical Research: Atmospheres, 123, 6196–6212, https://doi.org/10.1029/2017JD028033, 2018c.

McCluskey, C. S., DeMott, P. J., Ma, P.-L., and Burrows, S. M.: Numerical Representations of Marine Ice-Nucleating Particles in Remote Marine Environments Evaluated Against Observations, Geophysical Research Letters, 46, 7838–7847, https://doi.org/10.1029/2018GL081861, 2019.

McCluskey, C. S., Gettelman, A., Bardeen, C. G., DeMott, P. J., Moore, K. A., Kreidenweis, S. M., Hill, T. C. J., Barry, K. R., Twohy, C. H., Toohey, D. W., Rainwater, B., Jensen, J. B., Reeves, J. M., Alexander, S. P., and McFarquhar, G. M.: Simulating Southern Ocean Aerosol and Ice Nucleating Particles in the Community Earth System Model Version 2, Journal of Geophysical Research: Atmospheres, n/a, e2022JD036 955, https://doi.org/10.1029/2022JD036955, 2023.

McCoy, D. T., Burrows, S. M., Wood, R., Grosvenor, D. P., Elliott, S. M., Ma, P.-L., Rasch, P. J., and Hartmann, D. L.: Natural Aerosols Explain Seasonal and Spatial Patterns of Southern Ocean Cloud Albedo, Science Advances, 1, https://doi.org/10.1126/sciadv.1500157, 2015a.

McCoy, D. T., Hartmann, D. L., Zelinka, M. D., Ceppi, P., and Grosvenor, D. P.: Mixed-Phase Cloud Physics and Southern Ocean Cloud Feedback in Climate Models, Journal of Geophysical Research: Atmospheres, 120, 9539–9554, https://doi.org/10.1002/2015JD023603, 2015b.

McCoy, D. T., Tan, I., Hartmann, D. L., Zelinka, M. D., and Storelvmo, T.: On the Relationships among Cloud Cover, Mixed-Phase Partitioning, and Planetary Albedo in GCMs, Journal of Advances in Modeling Earth Systems, 8, 650–668, https://doi.org/10.1002/2015MS000589, 2016.

Meskhidze, N., Petters, M. D., Tsigaridis, K., Bates, T., O'Dowd, C., Reid, J., Lewis, E. R., Gantt, B., Anguelova, M. D., Bhave, P. V., Bird, J., Callaghan, A. H., Ceburnis, D., Chang, R., Clarke, A., de Leeuw, G., Deane, G., DeMott, P. J., Elliot, S., Facchini, M. C., Fairall, C. W., Hawkins, L., Hu, Y., Hudson, J. G., Johnson, M. S., Kaku, K. C., Keene, W. C., Kieber, D. J., Long, M. S., Mårtensson, M., Modini, R. L., Osburn, C. L., Prather, K. A., Pszenny, A., Rinaldi, M., Russell, L. M., Salter, M., Sayer, A. M., Smirnov, A., Suda, S. R., Toth, T. D.,

https://doi.org/10.5194/egusphere-2024-2159
Preprint. Discussion started: 25 July 2024

Worsnop, D. R., Wozniak, A., and Zorn, S. R.: Production Mechanisms, Number Concentration, Size Distribution, Chemical Composition, and Optical Properties of Sea Spray Aerosols, Atmospheric Science Letters, 14, 207–213, https://doi.org/10.1002/asl2.441, 2013.

Mitts, B. A., Wang, X., Lucero, D. D., Beall, C. M., Deane, G. B., DeMott, P. J., and Prather, K. A.: Importance of Supermicron Ice Nucleating Particles in Nascent Sea Spray, Geophysical Research Letters, 48, e2020GL089 633, https://doi.org/10.1029/2020GL089633, 2021.

Miyakawa, T., Taketani, F., Tobo, Y., Matsumoto, K., Yoshizue, M., Takigawa, M., and Kanaya, Y.: Measurements of Aerosol Particle Size Distributions and INPs Over the Southern Ocean in the Late Austral Summer of 2017 on Board the R/V Mirai: Importance of the Marine Boundary Layer Structure, Earth and Space Science, 10, e2022EA002 736, https://doi.org/10.1029/2022EA002736, 2023.

Modini, R. L., Frossard, A. A., Ahlm, L., Russell, L. M., Corrigan, C. E., Roberts, G. C., Hawkins, L. N., Schroder, J. C., Bertram, A. K., Zhao, R., Lee, A. K. Y., Abbatt, J. P. D., Lin, J., Nenes, A., Wang, Z., Wonaschütz, A., Sorooshian, A., Noone, K. J., Jonsson, H., Seinfeld, J. H., Toom-Sauntry, D., Macdonald, A. M., and Leaitch, W. R.: Primary Marine Aerosol-Cloud Interactions off the Coast of California, Journal of Geophysical Research: Atmospheres, 120, 4282–4303, https://doi.org/10.1002/2014JD022963, 2015.

Monahan, E. C. and Muircheartaigh, I.: Optimal Power-Law Description of Oceanic Whitecap Coverage Dependence on Wind Speed, Journal of Physical Oceanography, 10, 2094–2099, https://doi.org/10.1175/1520-0485(1980)010<2094:OPLDOO>2.0.CO;2, 1980.

Monahan, E. C., Spiel, D. E., and Davidson, K. L.: A Model of Marine Aerosol Generation Via Whitecaps and Wave Disruption, in: Oceanic Whitecaps: And Their Role in Air-Sea Exchange Processes, edited by Monahan, E. C. and Niocaill, G. M., Oceanographic Sciences Library, pp. 167–174, Springer Netherlands, Dordrecht, ISBN 978-94-009-4668-2, https://doi.org/10.1007/978-94-009-4668-2_16, 1986.

Moore, K. A.: Constraining Marine Ice Nucleating Particle Parameterizations in Atmospheric Models Using Observations from the Southern Ocean, MS Thesis, Colorado State University, https://mountainscholar.org/handle/10217/208435, 2020.

Moore, K. A., Alexander, S. P., Humphries, R. S., Jensen, J., Protat, A., Reeves, J. M., Sanchez, K. J., Kreidenweis, S. M., and DeMott, P. J.: Estimation of Sea Spray Aerosol Surface Area Over the Southern Ocean Using Scattering Measurements, Journal of Geophysical Research: Atmospheres, 127, e2022JD037 009, https://doi.org/10.1029/2022JD037009, 2022.

Moore, K. A., Hill, T. C. J., McCluskey, C. S., Twohy, C. H., Rainwater, B., Toohey, D. W., Sanchez, K. J., Kreidenweis, S. M., and DeMott, P. J.: Characterizing Ice Nucleating Particles Over the Southern Ocean Using Simultaneous Aircraft and Ship Observations, Journal of Geophysical Research: Atmospheres, 129, e2023JD039 543, https://doi.org/10.1029/2023JD039543, 2024.

Murphy, D. M. and Koop, T.: Review of the Vapour Pressures of Ice and Supercooled Water for Atmospheric Applications, Quarterly Journal of the Royal Meteorological Society, 131, 1539–1565, https://doi.org/10.1256/qj.04.94, 2005.

Naik, V., Szopa, S., Adhikary, B., Artaxo Netto, P. E., Berntsen, T., Collins, W. D., Fuzzi, S., Gallardo, L., Kiendler-Scharr, A., Klimont, Z., Liao, H., Unger, N., and Zanis, P.: Short-Lived Climate Forcers, in: Climate Change 2021: The Physical Science Basis. Contribution of Working Group I to the Sixth Assessment Report of the Intergovernmental Panel on Climate Change, edited by Masson-Delmotte, V., Zhai, P., Pirani, A., Connors, S. L., Péan, C., Berger, S., Caud, N., Chen, Y., Goldfarb, L., Gomis, M. I., Huang, M., Leitzell, K., Lonnoy, E., Matthews, J. B. R., Maycock, T. K., Waterfield, T., Yelekçi, Ö., Yu, R., and Zhou, B., pp. 817–922, Cambridge University Press, Cambridge, United Kingdom and New York, NY, USA, https://doi.org/10.1017/9781009157896.001, 2021.

Niemand, M., Möhler, O., Vogel, B., Vogel, H., Hoose, C., Connolly, P., Klein, H., Bingemer, H., DeMott, P. J., Skrotzki, J., and Leisner, T.: A Particle-Surface-Area-Based Parameterization of Immersion Freezing on Desert Dust Particles, Journal of the Atmospheric Sciences, 69, 3077–3092, https://doi.org/10.1175/JAS-D-11-0249.1, 2012.

Nilsson, E. D., Hultin, K. A. H., Mårtensson, E. M., Markuszewski, P., Rosman, K., and Krejci, R.: Baltic Sea Spray Emissions: In Situ Eddy Covariance Fluxes vs. Simulated Tank Sea Spray, Atmosphere, 12, 274, https://doi.org/10.3390/atmos12020274, 2021.

https://doi.org/10.5194/egusphere-2024-2159
Preprint. Discussion started: 25 July 2024

O'Dowd, C. D. and de Leeuw, G.: Marine Aerosol Production: A Review of the Current Knowledge, Philosophical Transactions of the Royal Society A: Mathematical, Physical and Engineering Sciences, 365, 1753–1774, https://doi.org/10.1098/rsta.2007.2043, 2007.

O'Dowd, C. D., Facchini, M. C., Cavalli, F., Ceburnis, D., Mircea, M., Decesari, S., Fuzzi, S., Yoon, Y. J., and Putaud, J.-P.: Biogenically Driven Organic Contribution to Marine Aerosol, Nature, 431, 676–680, https://doi.org/10.1038/nature02959, 2004.

Or, V. W., Estillore, A. D., Tivanski, A. V., and Grassian, V. H.: Lab on a Tip: Atomic Force Microscopy – Photothermal Infrared Spectroscopy of Atmospherically Relevant Organic/Inorganic Aerosol Particles in the Nanometer to Micrometer Size Range, Analyst, 143, 2765–2774, https://doi.org/10.1039/C8AN00171E, 2018.

O'Sullivan, D., Murray, B. J., Malkin, T. L., Whale, T. F., Umo, N. S., Atkinson, J. D., Price, H. C., Baustian, K. J., Browse, J., and Webb, M. E.: Ice Nucleation by Fertile Soil Dusts: Relative Importance of Mineral and Biogenic Components, Atmospheric Chemistry and Physics, 14, 1853–1867, https://doi.org/10.5194/acp-14-1853-2014, 2014.

Ovadnevaite, J., Manders, A., de Leeuw, G., Ceburnis, D., Monahan, C., Partanen, A.-I., Korhonen, H., and O'Dowd, C. D.: A Sea Spray Aerosol Flux Parameterization Encapsulating Wave State, Atmospheric Chemistry and Physics, 14, 1837–1852, https://doi.org/10.5194/acp-14-1837-2014, 2014.

Pierce, J. R. and Adams, P. J.: Global Evaluation of CCN Formation by Direct Emission of Sea Salt and Growth of Ultrafine Sea Salt, Journal of Geophysical Research: Atmospheres, 111, https://doi.org/10.1029/2005JD006186, 2006.

Prather, K. A., Bertram, T. H., Grassian, V. H., Deane, G. B., Stokes, M. D., DeMott, P. J., Aluwihare, L. I., Palenik, B. P., Azam, F., Seinfeld, J. H., Moffet, R. C., Molina, M. J., Cappa, C. D., Geiger, F. M., Roberts, G. C., Russell, L. M., Ault, A. P., Baltrusaitis, J., Collins, D. B., Corrigan, C. E., Cuadra-Rodriguez, L. A., Ebben, C. J., Forestieri, S. D., Guasco, T. L., Hersey, S. P., Kim, M. J., Lambert, W. F., Modini, R. L., Mui, W., Pedler, B. E., Ruppel, M. J., Ryder, O. S., Schoepp, N. G., Sullivan, R. C., and Zhao, D.: Bringing the Ocean into the Laboratory to Probe the Chemical Complexity of Sea Spray Aerosol, Proceedings of the National Academy of Sciences, 110, 7550–7555, https://doi.org/10.1073/pnas.1300262110, 2013.

Pummer, B. G., Budke, C., Augustin-Bauditz, S., Niedermeier, D., Felgitsch, L., Kampf, C. J., Huber, R. G., Liedl, K. R., Loerting, T., Moschen, T., Schauperl, M., Tollinger, M., Morris, C. E., Wex, H., Grothe, H., Pöschl, U., Koop, T., and Fröhlich-Nowoisky, J.: Ice Nucleation by Water-Soluble Macromolecules, Atmospheric Chemistry and Physics, 15, 4077–4091, https://doi.org/10.5194/acp-15-4077-2015, 2015.

Quinn, P. K., Coffman, D. J., Johnson, J. E., Upchurch, L. M., and Bates, T. S.: Small Fraction of Marine Cloud Condensation Nuclei Made up of Sea Spray Aerosol, Nature Geoscience, 10, 674–679, https://doi.org/10.1038/ngeo3003, 2017.

Raatikainen, T., Prank, M., Ahola, J., Kokkola, H., Tonttila, J., and Romakkaniemi, S.: The Effect of Marine Ice-Nucleating Particles on Mixed-Phase Clouds, Atmospheric Chemistry and Physics, 22, 3763–3778, https://doi.org/10.5194/acp-22-3763-2022, 2022.

Raman, A., Hill, T., DeMott, P. J., Singh, B., Zhang, K., Ma, P.-L., Wu, M., Wang, H., Alexander, S. P., and Burrows, S. M.: Long-Term Variability in Immersion-Mode Marine Ice-Nucleating Particles from Climate Model Simulations and Observations, Atmospheric Chemistry and Physics, 23, 5735–5762, https://doi.org/10.5194/acp-23-5735-2023, 2023.

Ray, K. K., Lee, H. D., Gutierrez, M. A. J., Chang, F. J., and Tivanski, A. V.: Correlating 3D Morphology, Phase State, and Viscoelastic Properties of Individual Substrate-Deposited Particles, Analytical Chemistry, 91, 7621–7630, https://doi.org/10.1021/acs.analchem.9b00333, 2019.

Rogers, D. C.: Development of a Continuous Flow Thermal Gradient Diffusion Chamber for Ice Nucleation Studies, Atmospheric Research, 22, 149–181, https://doi.org/10.1016/0169-8095(88)90005-1, 1988.

https://doi.org/10.5194/egusphere-2024-2159
Preprint. Discussion started: 25 July 2024

Rogers, D. C., DeMott, P. J., Kreidenweis, S. M., and Chen, Y.: A Continuous-Flow Diffusion Chamber for Airborne Measurements of Ice Nuclei, Journal of Atmospheric and Oceanic Technology, 18, 17, 2001.

Rosinski, J., Haagenson, P. L., Nagamoto, C. T., and Parungo, F.: Nature of Ice-Forming Nuclei in Marine Air Masses, Journal of Aerosol Science, 18, 291–309, https://doi.org/10.1016/0021-8502(87)90024-3, 1987.

Saliba, G., Chen, C.-L., Lewis, S., Russell, L. M., Rivellini, L.-H., Lee, A. K. Y., Quinn, P. K., Bates, T. S., Haëntjens, N., Boss, E. S., Karp-Boss, L., Baetge, N., Carlson, C. A., and Behrenfeld, M. J.: Factors Driving the Seasonal and Hourly Variability of Sea-Spray Aerosol Number in the North Atlantic, Proceedings of the National Academy of Sciences, 116, 20 309–20 314, https://doi.org/10.1073/pnas.1907574116, 2019.

Salter, M. E., Nilsson, E. D., Butcher, A., and Bilde, M.: On the Seawater Temperature Dependence of the Sea Spray Aerosol Generated by a Continuous Plunging Jet, Journal of Geophysical Research: Atmospheres, 119, 9052–9072, https://doi.org/10.1002/2013JD021376, 2014.

Salter, M. E., Zieger, P., Acosta Navarro, J. C., Grythe, H., Kirkevåg, A., Rosati, B., Riipinen, I., and Nilsson, E. D.: An Empirically Derived Inorganic Sea Spray Source Function Incorporating Sea Surface Temperature, Atmospheric Chemistry and Physics, 15, 11 047–11 066, https://doi.org/10.5194/acp-15-11047-2015, 2015.

Sauer, J. S., Mayer, K. J., Lee, C., Alves, M. R., Amiri, S., Bahaveolos, C. J., Franklin, E. B., Crocker, D. R., Dang, D., Dinasquet, J., Garofalo, L. A., Kaluarachchi, C. P., Kilgour, D. B., Mael, L. E., Mitts, B. A., Moon, D. R., Moore, A. N., Morris, C. K., Mullenmeister, C. A., Ni, C.-M., Pendergraft, M. A., Petras, D., Simpson, R. M. C., Smith, S., Tumminello, P. R., Walker, J. L., DeMott, P. J., Farmer, D. K., Goldstein, A. H., Grassian, V. H., Jaffe, J. S., Malfatti, F., Martz, T. R., Slade, J. H., Tivanski, A. V., Bertram, T. H., Cappa, C. D., and Prather, K. A.: The Sea Spray Chemistry and Particle Evolution Study (SeaSCAPE): Overview and Experimental Methods, Environmental Science: Processes & Impacts, 24, 290–315, https://doi.org/10.1039/D1EM00260K, 2022.

Schmale, J., Baccarini, A., Thurnherr, I., Henning, S., Efraim, A., Regayre, L., Bolas, C., Hartmann, M., Welti, A., Lehtipalo, K., Aemisegger, F., Tatzelt, C., Landwehr, S., Modini, R. L., Tummon, F., Johnson, J. S., Harris, N., Schnaiter, M., Toffoli, A., Derkani, M., Bukowiecki, N., Stratmann, F., Dommen, J., Baltensperger, U., Wernli, H., Rosenfeld, D., Gysel-Beer, M., and Carslaw, K. S.: Overview of the Antarctic Circumnavigation Expedition: Study of Preindustrial-like Aerosols and Their Climate Effects (ACE-SPACE), Bulletin of the American Meteorological Society, 100, 2260–2283, https://doi.org/10.1175/BAMS-D-18-0187.1, 2019.

Schnell, R. C. and Vali, G.: Biogenic Ice Nuclei: Part I. Terrestrial and Marine Sources, Journal of the Atmospheric Sciences, 33, 1554–1564, https://doi.org/10.1175/1520-0469(1976)033<1554:BINPIT>2.0.CO;2, 1976.

Schwier, A. N., Sellegri, K., Mas, S., Charrière, B., Pey, J., Rose, C., Temime-Roussel, B., Jaffrezo, J.-L., Parin, D., Picard, D., Ribeiro, M., Roberts, G., Sempéré, R., Marchand, N., and D'Anna, B.: Primary Marine Aerosol Physical Flux and Chemical Composition during a Nutrient Enrichment Experiment in Mesocosms in the Mediterranean Sea, Atmospheric Chemistry and Physics, 17, 14 645–14 660, https://doi.org/10.5194/acp-17-14645-2017, 2017.

Sellegri, K., O'Dowd, C. D., Yoon, Y. J., Jennings, S. G., and de Leeuw, G.: Surfactants and Submicron Sea Spray Generation, Journal of Geophysical Research: Atmospheres, 111, https://doi.org/10.1029/2005JD006658, 2006.

Sellegri, K., Barthelmeß, T., Trueblood, J., Cristi, A., Freney, E., Rose, C., Barr, N., Harvey, M., Safi, K., Deppeler, S., Thompson, K., Dillon, W., Engel, A., and Law, C.: Quantified Effect of Seawater Biogeochemistry on the Temperature Dependence of Sea Spray Aerosol Fluxes, Atmospheric Chemistry and Physics, 23, 12 949–12 964, https://doi.org/10.5194/acp-23-12949-2023, 2023.

Sofiev, M., Soares, J., Prank, M., de Leeuw, G., and Kukkonen, J.: A Regional-to-Global Model of Emission and Transport of Sea Salt Particles in the Atmosphere, Journal of Geophysical Research: Atmospheres, 116, https://doi.org/10.1029/2010JD014713, 2011.

https://doi.org/10.5194/egusphere-2024-2159
Preprint. Discussion started: 25 July 2024

Steinke, I., DeMott, P. J., Deane, G. B., Hill, T. C. J., Maltrud, M., Raman, A., and Burrows, S. M.: A Numerical Framework for Simulating the Atmospheric Variability of Supermicron Marine Biogenic Ice Nucleating Particles, Atmospheric Chemistry and Physics, 22, 847–859, https://doi.org/10.5194/acp-22-847-2022, 2022.

Stokes, M. D., Deane, G. B., Prather, K., Bertram, T. H., Ruppel, M. J., Ryder, O. S., Brady, J. M., and Zhao, D.: A Marine Aerosol Reference Tank System as a Breaking Wave Analogue for the Production of Foam and Sea-Spray Aerosols, Atmospheric Measurement Techniques, 6, 1085–1094, https://doi.org/10.5194/amt-6-1085-2013, 2013.

Suski, K. J., Hill, T. C. J., Levin, E. J. T., Miller, A., DeMott, P. J., and Kreidenweis, S. M.: Agricultural Harvesting Emissions of Ice-Nucleating Particles, Atmospheric Chemistry and Physics, 18, 13 755–13 771, https://doi.org/10.5194/acp-18-13755-2018, 2018.

Tang, I. N., Tridico, A. C., and Fung, K. H.: Thermodynamic and Optical Properties of Sea Salt Aerosols, Journal of Geophysical Research: Atmospheres, 102, 23 269–23 275, https://doi.org/10.1029/97JD01806, 1997.

Tatzelt, C., Henning, S., Welti, A., Baccarini, A., Hartmann, M., Gysel-Beer, M., van Pinxteren, M., Modini, R. L., Schmale, J., and Stratmann, F.: Circum-Antarctic Abundance and Properties of CCN and INPs, Atmospheric Chemistry and Physics, 22, 9721–9745, https://doi.org/10.5194/acp-22-9721-2022, 2022.

Tobo, Y., Prenni, A. J., DeMott, P. J., Huffman, J. A., McCluskey, C. S., Tian, G., Pöhlker, C., Pöschl, U., and Kreidenweis, S. M.: Biological Aerosol Particles as a Key Determinant of Ice Nuclei Populations in a Forest Ecosystem, Journal of Geophysical Research: Atmospheres, 118, 10,100–10,110, https://doi.org/10.1002/jgrd.50801, 2013.

Ullrich, R., Hoose, C., Möhler, O., Niemand, M., Wagner, R., Höhler, K., Hiranuma, N., Saathoff, H., and Leisner, T.: A New Ice Nucleation Active Site Parameterization for Desert Dust and Soot, Journal of the Atmospheric Sciences, 74, 699–717, https://doi.org/10.1175/JAS-D-16-0074.1, 2017.

Vali, G.: Quantitative Evaluation of Experimental Results on the Heterogeneous Freezing Nucleation of Supercooled Liquids, Journal of the Atmospheric Sciences, 28, 402–409, https://doi.org/10.1175/1520-0469(1971)028<0402:QEOERA>2.0.CO;2, 1971.

van Pinxteren, M., Fomba, K. W., Triesch, N., Stolle, C., Wurl, O., Bahlmann, E., Gong, X., Voigtländer, J., Wex, H., Robinson, T.-B., Barthel, S., Zeppenfeld, S., Hoffmann, E. H., Roveretto, M., Li, C., Grosselin, B., Daële, V., Senf, F., van Pinxteren, D., Manzi, M., Zabalegui, N., Frka, S., Gašparović, B., Pereira, R., Li, T., Wen, L., Li, J., Zhu, C., Chen, H., Chen, J., Fiedler, B., von Tümpling, W., Read, K. A., Punjabi, S., Lewis, A. C., Hopkins, J. R., Carpenter, L. J., Peeken, I., Rixen, T., Schulz-Bull, D., Monge, M. E., Mellouki, A., George, C., Stratmann, F., and Herrmann, H.: Marine Organic Matter in the Remote Environment of the Cape Verde Islands – an Introduction and Overview to the MarParCloud Campaign, Atmospheric Chemistry and Physics, 20, 6921–6951, https://doi.org/10.5194/acp-20-6921-2020, 2020.

Verdugo, P.: Marine Microgels, Annual Review of Marine Science, 4, 375–400, https://doi.org/10.1146/annurev-marine-120709-142759, 2012.

Vergara-Temprado, J., Murray, B. J., Wilson, T. W., O'Sullivan, D., Browse, J., Pringle, K. J., Ardon-Dryer, K., Bertram, A. K., Burrows, S. M., Ceburnis, D., DeMott, P. J., Mason, R. H., O'Dowd, C. D., Rinaldi, M., and Carslaw, K. S.: Contribution of Feldspar and Marine Organic Aerosols to Global Ice Nucleating Particle Concentrations, Atmospheric Chemistry and Physics, 17, 3637–3658, https://doi.org/10.5194/acp-17-3637-2017, 2017.

Vergara-Temprado, J., Miltenberger, A. K., Furtado, K., Grosvenor, D. P., Shipway, B. J., Hill, A. A., Wilkinson, J. M., Field, P. R., Murray, B. J., and Carslaw, K. S.: Strong Control of Southern Ocean Cloud Reflectivity by Ice-Nucleating Particles, Proceedings of the National Academy of Sciences, 115, 2687–2692, https://doi.org/10.1073/pnas.1721627115, 2018.

https://doi.org/10.5194/egusphere-2024-2159
Preprint. Discussion started: 25 July 2024

Villefer, A., Benoit, M., Violeau, D., Luneau, C., and Branger, H.: Influence of Following, Regular, and Irregular Long Waves on Wind-Wave Growth with Fetch: An Experimental Study, Journal of Physical Oceanography, 51, 3435–3448, https://doi.org/10.1175/JPO-D-21-0050.1, 2021.

Vollestad, P. and Jensen, A.: Modification of Airflow Structure Due to Wave Breaking on a Submerged Topography, Boundary-Layer Meteorology, 180, 507–526, https://doi.org/10.1007/s10546-021-00631-3, 2021.

von der Weiden, S.-L., Drewnick, F., and Borrmann, S.: Particle Loss Calculator – a New Software Tool for the Assessment of the Performance of Aerosol Inlet Systems, Atmospheric Measurement Techniques, 2, 479–494, https://doi.org/10.5194/amt-2-479-2009, 2009.

Wang, X., Sultana, C. M., Trueblood, J., Hill, T. C. J., Malfatti, F., Lee, C., Laskina, O., Moore, K. A., Beall, C. M., McCluskey, C. S., Cornwell, G. C., Zhou, Y., Cox, J. L., Pendergraft, M. A., Santander, M. V., Bertram, T. H., Cappa, C. D., Azam, F., DeMott, P. J., Grassian, V. H., and Prather, K. A.: Microbial Control of Sea Spray Aerosol Composition: A Tale of Two Blooms, ACS Central Science, 1, 124–131, https://doi.org/10.1021/acscentsci.5b00148, 2015.

Welti, A., Müller, K., Fleming, Z. L., and Stratmann, F.: Concentration and Variability of Ice Nuclei in the Subtropical Maritime Boundary Layer, Atmospheric Chemistry and Physics, 18, 5307–5320, https://doi.org/10.5194/acp-18-5307-2018, 2018.

Welti, A., Bigg, E. K., DeMott, P. J., Gong, X., Hartmann, M., Harvey, M., Henning, S., Herenz, P., Hill, T. C. J., Hornblow, B., Leck, C., Löffler, M., McCluskey, C. S., Rauker, A. M., Schmale, J., Tatzelt, C., van Pinxteren, M., and Stratmann, F.: Ship-Based Measurements of Ice Nuclei Concentrations over the Arctic, Atlantic, Pacific and Southern Oceans, Atmospheric Chemistry and Physics, 20, 15 191–15 206, https://doi.org/10.5194/acp-20-15191-2020, 2020.

Wilbourn, E. K., Thornton, D. C. O., Ott, C., Graff, J., Quinn, P. K., Bates, T. S., Betha, R., Russell, L. M., Behrenfeld, M. J., and Brooks, S. D.: Ice Nucleation by Marine Aerosols Over the North Atlantic Ocean in Late Spring, Journal of Geophysical Research: Atmospheres, 125, e2019JD030 913, https://doi.org/10.1029/2019JD030913, 2020.

Wilson, T. W., Ladino, L. A., Alpert, P. A., Breckels, M. N., Brooks, I. M., Browse, J., Burrows, S. M., Carslaw, K. S., Huffman, J. A., Judd, C., Kilthau, W. P., Mason, R. H., McFiggans, G., Miller, L. A., Nájera, J. J., Polishchuk, E., Rae, S., Schiller, C. L., Si, M., Temprado, J. V., Whale, T. F., Wong, J. P. S., Wurl, O., Yakobi-Hancock, J. D., Abbatt, J. P. D., Aller, J. Y., Bertram, A. K., Knopf, D. A., and Murray, B. J.: A Marine Biogenic Source of Atmospheric Ice-Nucleating Particles, Nature, 525, 234–238, https://doi.org/10.1038/nature14986, 2015.

Zábori, J., Matisāns, M., Krejci, R., Nilsson, E. D., and Ström, J.: Artificial Primary Marine Aerosol Production: A Laboratory Study with Varying Water Temperature, Salinity, and Succinic Acid Concentration, Atmospheric Chemistry and Physics, 12, 10 709–10 724, https://doi.org/10.5194/acp-12-10709-2012, 2012.

Zavadsky, A. and Shemer, L.: Characterization of Turbulent Airflow over Evolving Water-Waves in a Wind-Wave Tank, Journal of Geophysical Research: Oceans, 117, https://doi.org/10.1029/2011JC007790, 2012.

Zelinka, M. D., Myers, T. A., McCoy, D. T., Po-Chedley, S., Caldwell, P. M., Ceppi, P., Klein, S. A., and Taylor, K. E.: Causes of Higher Climate Sensitivity in CMIP6 Models, Geophysical Research Letters, 47, e2019GL085 782, https://doi.org/10.1029/2019GL085782, 2020.

Zhao, X., Liu, X., Burrows, S. M., and Shi, Y.: Effects of Marine Organic Aerosols as Sources of Immersion-Mode Ice-Nucleating Particles on High-Latitude Mixed-Phase Clouds, Atmospheric Chemistry and Physics, 21, 2305–2327, https://doi.org/10.5194/acp-21-2305-2021, 2021.

Zieger, P., Väisänen, O., Corbin, J. C., Partridge, D. G., Bastelberger, S., Mousavi-Fard, M., Rosati, B., Gysel, M., Krieger, U. K., Leck, C., Nenes, A., Riipinen, I., Virtanen, A., and Salter, M. E.: Revising the Hygroscopicity of Inorganic Sea Salt Particles, Nature Communications, 8, 15 883, https://doi.org/10.1038/ncomms15883, 2017.

https://doi.org/10.5194/egusphere-2024-2159
Preprint. Discussion started: 25 July 2024

Zinke, J., Nilsson, E. D., Zieger, P., and Salter, M. E.: The Effect of Seawater Salinity and Seawater Temperature on Sea Salt Aerosol
1005 Production, Journal of Geophysical Research: Atmospheres, 127, e2021JD036 005, https://doi.org/10.1029/2021JD036005, 2022.